TARGETING THE MITOCHONDRIAL PYRUVATE COMPLEX TO ALTER METABOLIC PROGRAMMING IN PANCREATIC DUCTAL ADENOCARCINOMA

by

Hassan Asif Ali

B.Sc., University of British Columbia, 2019

A THESIS SUBMITTED IN PARTIAL FULFILLMENT OF
THE REQUIREMENTS FOR THE DEGREE OF

MASTER OF SCIENCE

in

The Faculty of Graduate and Postdoctoral Studies

(Interdisciplinary Oncology)

THE UNIVERSITY OF BRITISH COLUMBIA

(Vancouver)

August 2022

The following individuals certify that they have read, and recommend to the Faculty of Graduate and Postdoctoral Studies for acceptance, the thesis entitled:

Targeting the Mitochondrial Pyruvate Complex to Alter Metabolic Programming in Pancreatic Cancer

submitted by Hassan Asif Ali in partial fulfillment of the requirements for the degree of Master of Science in Interdisciplinary Oncology

Examining Committee:

David Schaeffer, Associate Professor, Pathology and Laboratory Medicine, UBC
Co-supervisor

Daniel Renouf, Associate Professor, Medical Oncology, UBC
Co-supervisor

James Johnson, Professor, Cellular and Physiological Sciences, UBC
Supervisory Committee Member

Kasmintan Schrader, Assistant Professor, Medical Genetics, UBC
Additional Examiner

Additional Supervisory Committee Members:

Francis Lynn, Associate Professor, Cellular and Physiological Sciences, UBC
Supervisory Committee Member

Marcel Bally, Professor, Pathology and Laboratory Medicine, UBC
Supervisory Committee Member

Abstract

Pancreatic ductal adenocarcinoma (PDAC) can be stratified into distinct transcriptome based molecular subtypes, with the 'basal-like' (or 'squamous') subtype being associated with worse prognosis, compared to the 'classical' subtype. These subtypes are assigned based on Moffitt genes signature scores where scores above a threshold value are indictive of the basal-like subtype. Furthermore, PDAC tumours have unique metabolic transcriptomic profiles based on stratification of glycolytic and cholesterogenic genes which correlate with basal-like and classical gene expression patterns, respectively. The mitochondrial pyruvate complex (MPC) mediates the transport of pyruvate into the mitochondria. The mitochondrial pyruvate carrier 1 (MPC1) gene, which encodes one of two subunits of MPC, is deleted in over 60% of metastatic PDAC and PDAC glycolytic tumours have lowest levels of MPC1 expression. Using PDAC tissue microarray data, our group found that reduced MPC1 protein expression correlates with reduced survival in patients. Therefore, we hypothesized that targeting MPC1 will alter metabolic reprogramming which may modulate tumour aggressiveness in tumour models. Genomically and clinically annotated patient-derived tumour organoids (PDOs) were generated from metastatic biopsies from patients enrolled in the PanGen study. Baseline metabolism and metabolic flux were measured using Seahorse XFe96 based glycolytic and mito stress tests, these tests were adapted for compatibility with PDOs. Baseline glycolysis and oxidative phosphorylation (OXPHOS) rates demonstrated high variability in glycolytic reserves highlighting the extent of metabolic reprogramming in PDOs. This variability in glycolytic reserve positively associated with Moffitt gene signature scores where PDOs with larger reserves tended to have higher Moffitt scores. To alter metabolic activity, eight PDOs were treated for

48 hours with UK-5099, a MPC1 inhibitor, or SRT-1720. SRT-1720 is an activator of sirtuin 1 (SIRT1) which deacetylates peroxisome proliferator-activated receptor gamma coactivator 1-alpha (PGC1α), enhancing its activity. PGC1α has been shown to increase transcription of MPC1. Treatment with UK-5099 raised glycolysis and glycolytic capacity in four PDOs tested and reduced maximal respiration rates in seven PDOs. Treatment with SRT-1720 reduced glycolytic capacity in two PDOs but did not alter OXPHOS rates. Taken together, these results elicit the variability in metabolic dependency in PDOs to meet energy demands and the plasticity of metabolic reprogramming.

Lay Summary

Pancreatic cancer is the third leading cause of cancer related deaths with the lowest survival rates amongst all solid tumours. Pancreatic tumours change their metabolism to reduce pathways limiting them from growing faster and spreading. One such pathway is oxidative phosphorylation (OXPHOS), one of two sources of a cells energy. OXPHOS is limited by reducing levels of mitochondrial pyruvate carrier 1 (MPC1) protein which delivers fuel for this process. Glycolysis, the other energy producing pathway, creates this fuel and is greatly increased. Here, We used patient derived organoids (PDOs), which are mini tumour models, to show that tumours which are able to increase glycolysis to a greater extent associate with a tumour group known to be more aggressive and have the poorest treatment response. We show the possibility of therapeutically shifting metabolism by using MPC1 targeting agents and lay the groundwork to identify agents that increase MPC1/OXPHOS in PDOs.

Preface

This thesis contains work on samples obtained through the PanGen project (NCT02869802) approved by the BC Cancer Research Ethics Board (H16-00291). Whole genome and transcriptome sequencing was performed at the Canada's Michael Smith Genome Sciences Centre at BC Cancer. The project was conceptualized and study was designed by myself, Dr. Joanna Karasinska, Dr. Daniel Renouf and Dr. David Schaeffer. I was primarily responsible for data generation, analysis and interpretation of findings. Organoid development was a joint effort between myself, Andrew Metcalfe and Dr.Joanna Karasinska. Viability studies were carried out with the guidance of Dr. Joanna Karasinska, Cassia Warren and Andrew Metcalfe. I performed all bioinformatic analyses with assistance from James Topham. All seahorse assays were done by me with guidance from Cassia Warren and Dr. Shawn Chafe.

Table of Contents

List of Tables

List of Figures

List of Abbreviations

2D	two dimension
ADEX	aberrantly differentiated endocrine exocrine
CA-IX	carbonic anhydrase IX
CAFs	cancer associated fibroblasts
CGM	complete growth media
CT	computed tomography
DMSO	dimethyl sulfoxide
ECAR	extracellular acidification rate
ECM	extra-cellular matrix
EMT	epithelial to mesenchymal transition
ETC	electron transport chain
FAP	fibroblast activation protein
FCCP	carbonyl cyanide-4-(trifluoromethoxy) phenylhydrazone
GM-CSF	granulocyte-macrophage colony-stimulating factor
MPC	mitochondrial pyruvate complex
MPC1	mitochondrial pyruvate carrier 1
MPC2	mitochondrial pyruvate carrier 2
mPDO	metastatic Patient derived organoid
NCCN	National Comprehensive Cancer Network
OCR	oxygen consumption rate
OXPHOS	oxidative phosphorylation
PanIN	pancreatic intraepithelial neoplasms

PARP	poly(adenosine diphosphate-ribose) polymerase
PDAC	pancreatic ductal adenocarcinoma
PDOs	Patient derived organoids
PGC1α	peroxisome proliferator-activated receptor gamma coactivator 1-alpha
PNETs	pancreatic neuroendocrine tumours
SIRT1	sirtuin 1
TCA	tricarboxylic acid

Acknowledgements

I am truly grateful to my supervisors Dr. David Schaeffer and Dr. Daniel Renouf for their guidance and mentorship thoughtout my graduate studies and prior, as an undergraduate. Thank you for giving me the opportunity to learn and contribute to the field of oncology. My sincerest thanks to Dr.Joanna Karasinska for her guidance, encouragement and for constantly challenging me to think critically. I would also like to thank my thesis advisory committee members, Dr. James Johnson, Dr. Francis Lynn and Dr. Marcel Bally for their insights, valuable feedback and criticisms. Thank you to Cassia Warren, for her mentorship and support; James Topham, for his bioinformatics expertise and comradery; and Andrew Metcalfe, for his technical expertise and assistance. I would like to thank our co-ops, Nathan Perillat and Anthony Miyagi for their daily help. Thank you to all other members of Pancreas Centre BC for their support during this endeavour.

Thank you to the Department of Experimental Therapeutics and associated members for their assistance and access to resources. A profound thank you to all those who contributed to PanGen, especially the participants. I would also like to thank all colleagues at the BC Cancer Research Centre. Thank you to the interdisciplinary oncology program and to my fellow IOP colleagues for their support.

My warmest thank you to my family for their unwavering support and constant encouragement throughout my endeavours. Lastly a tremendous thank you to all my friends for all the support, adventures and incredible memories.

Dedication

To my family and friends like family, without whom none of this would be possible.

Chapter 1: Introduction

1.1 Pancreatic Cancer

1.1.1 *Global health Burden*

Pancreatic cancer encompasses an array of malignancies arising from its exocrine and endocrine compartments. The most common form is pancreatic ductal adenocarcinoma (PDAC), representing approximately 95% of all pancreatic cancer patients, while other less frequent types of exocrine variants include squamous cell carcinomas, adenosquamous carcinomas, signet ring cell carcinomas, undifferentiated carcinomas and undifferentiated carcinomas with osteoclastic giant cells. Pancreatic cancers with an endocrine origin are primarily comprised of pancreatic neuroendocrine tumours (PNETs) which represent ~5% of all malignancies [1]. In 2021, 6,700 new patients with pancreatic cancer were registered in Canada, representing 2.9% of all cancers, an 11.7% increase in incidence compared to 2020 [2]. The United States estimates 62,210 new patients in 2022, representing 3.2% of all new cancers [3]. The risk of developing pancreatic cancer increases with age. The incidence rate is highest for individuals over 70 years with diagnosis rare for those below 55 years [4]. Aside from age; obesity and diabetes are emerging as catalysts of disease onset [5]. Despite low incidence rates, pancreatic cancer ranks amongst the most lethal malignancies. It has a one-year survival rate of 20% [6] and a 5-year survival rate of 10% [2] making it the third leading cause of cancer related mortalities. Factors effecting high mortality and increased disease burden include late detection [5], high recurrence rates [7], lack of clinically actionable biomarkers [8], intertumoral and intratumoral genomic and transcriptomic heterogeneity [9] and

resistance to treatment [10]. The primary focus of this thesis is on PDAC.

1.1.2 *Risk factors*

Modifiable and environmental factors include (1) tobacco use which induces genetic mutations (*KRAS*, *P53*) amongst other traumas accounting for 20-35% of all patients [6], (2) high alcohol consumption, with an excess of three daily drinks raising relative risk from 1.22 to 1.36, (3) obesity, a 5kg/m2 rise in body mass index (BMI) can raise the relative risk by 1.12, (4) chronic pancreatitis, patients have an eight-fold increased risk of PDAC five years after diagnosis [6, 11], and (5) type II diabetes, long term diabetic patients have a 1.5-2 fold increased risk [5, 12]. Hyperinsulinemia is independently associated with PDAC incidence and it has been shown that a moderate decrease in endogenous insulin leads to a 50% reduction in pre-cancerous lesions [13, 14]. Insulin resistance forms, such as type 3c diabetes mellitus caused by chronic pancreatitis, further raises the risk of developing PDAC (HR=33.5) [15]. Unmodifiable, hereditary risk factors include hereditary breast and ovarian cancer syndrome, these cause 17-19% of hereditary tumours especially in BRCA2 mutated conditions; Lynch syndrome, microsatellite instability increases predisposition to PDAC (RR=8.6); Peutz-Jeghers syndrome, STKll/LKB1 mutations give rise to gastrointestinal neoplasia's (RR=132); and hereditary pancreatitis, owing to chronic inflammation can cause onset at childhood (RR=69) [7].

1.1.3 *Resectable vs non-resectable PDAC*

Conventionally, PDAC can be classified into resectable, borderline resectable, locally advanced unresectable and metastatic stages. At presentation, approximately 15-20%

of patients are eligible for resection. Eligibility criteria for surgical resection as defined by the National Comprehensive Cancer Network (NCCN) include no visible blood vessel involvement or less than a 180º circumference contact with the superior mesenteric vein or portal vein without vein contour irregularity [16]. Major blood vessel involvement occurs in approximately 30-40% of patients [17]. If major arteries are involved but venous contour is preserved these tumours are considered borderline resectable. Despite surgical resection, mortality occurs in more than 80% of patients owing to local recurrence and/or distant metastasis [18]. Approximately 30% of those who undergo a complete resection survive 5 years while survival is even lower for those with margin positive resections [18, 19]. The five-year survival rate for all resectable patients is 15-20% [2]. Tumours encasing (>180º vessel circumference contact) adjacent arteries or where venous contour is unpreserved are considered locally advanced unresectable [19]. Prognosis for these patients is dismal where about 60% eventually develop metastatic disease and about 40% die of complications related to progression (e.g. bleeding and perforation) [16, 20]. The five-year survival rate for locally advanced patients is 11% [2]. However, 10-35% [21] locally advanced tumours can be converted to resectable tumours with neoadjuvant chemotherapy potentially allowing for curative resection [21, 22]. Metastasis occurs in over half of all patients [16]. Metastasis type can be considered 'peritoneal' if site of metastasis is limited to the peritoneum; 'lymph node involved' if intra-abdominal metastasis occurs; and 'distant' if lung, liver, bone or other distant metastasis occur [20]. Survival even with systemic therapy remains less than a year for metastatic disease [16] with only 2% of patients surviving five years [2].

1.1.4 *Pathology*

The majority of PDACs are found in the head of the pancreas with rare body and tail involvement. In 2000, more than two decades ago, Hruban et al. [23] proposed that pancreatic carcinogenesis progresses stepwise beginning with macroscopic and microscopic precursors. Macroscopic precursors include with mucinous cystic neoplasms (MCN) and intraductal mucinous neoplasia's (IPMN), whereas microscopic precursors include atypical flat lesions and pancreatic intraepithelial neoplasms (PanIN)s. PanIN development starts with molecular changes such as telomere shortening and accumulation of driver mutations in the oncogene KRAS, followed by loss in expression of cyclin D1 and p16/CDKN2A function and ultimately changes in p53 expression, loss of SMAD4/DPC4 and BRCA2 [24, 25]. Although both microscopic precursors have ductal origin, acinar cells have also been shown to give rise to PanIN and atypical flat lesions via a process called acinar-to-ductal metaplasia which can occur due to abnormal expression of the ductal gene SOX9 [26, 27]. More recently, in 2016 Notta et al. [23] proposed a new catastrophic failure model where a single catastrophic event causes multiple driver events [28]. These large-scale gene disruption and complex chromosomal rearrangements result in punctuated tumour evolution [28, 29, 30]; most CNVs arise from individual chromothripsis events and that two or more somatic alterations required for PDAC development/progression can occur concurrently. These mutational phenomena result in a rapid rather than gradual development of PDAC [23].

1.1.5 *Pancreatic tumour microenvironment*

Desmoplasia, characterized by a fibrotic stroma is a histologic hallmark of PDAC in the majority of tumours. Stromal cells such as cancer associated fibroblasts (CAFs), endothelial cells, stellate cells and immune cells; create a mechanical barrier around the tumour via fibrotic stromal deposition. The fibroblastic population can comprise up to 90% of tumour mass [31]. Once activated, this stroma dynamically contributes to proliferation and invasion efforts by the tumour and influences metastasis. CAFs have been shown to provide metabolic aid to cancer cells to influence energy production via glycolysis over aerobic respiration thereby inducing the Warburg effect, where tumour metabolism is reprogrammed to prefer glycolysis despite being in a normoxic state. A sub-population of CAFs called cancer-associated mesenchymal stem cells induce invasion by producing granulocyte-macrophage colony-stimulating factor (GM-CSF) which downregulates the adhesion protein E-cadherin and upregulates vimentin, a marker of epithelial to mesenchymal transition (EMT) [32]. The dense mechanical barrier generates stress and obstructs lymphatic flow resulting in increased interstitial fluid pressure which leads to vascular compression, reduction in tissue perfusion and internal hypoxic conditions, conferring chemoresistance to first line systemic therapies such as Gemcitabine [33]. The stroma also prevents effective immune infiltration and even inhibits both innate and adaptive immune systems by reducing CD8 T cells and; increasing M2 macrophages, N2 neutrophils and T-regulatory cells in the tumour microenvironment [33, 34]. However, stromal depletion leads to a more aggressive form of PDAC suggesting a restraining, rather than supporting role. Ozdemir et al. showed that myofibroblast (α-SMA positive CAFs) depletion gave rise to undifferentiated and invasive tumours with necrotic regions. These tumours showed increased EMT, induced a stem-cell like phenotype and increased in vivo tumourgenicity. Myofibroblast

depletion at the PanIN or metastatic stage reduced angiogenesis while not altering glycolysis thereby enhancing tumour hypoxia [35]. Similarly, Rhim et al. showed stromal depletion via sonic hedgehog inhibition enhanced proliferation and resulted in earlier metastasis with more undifferentiated tumours consequently resulting in reduced survival [35, 36, 37]. Taken together, it is evident that the stroma plays an incredibly complex role in PDAC pathogenesis.

1.1.6 *Diagnosis and evolution of treatment*

The majority (>80%) of patients present with locally advanced or metastatic, and therefore non-resectable, disease. Symptoms can be non-specific such as abdominal pain, fatigue, unexpected weight loss and poor appetite; those such as jaundice, dark urine and light-colored stool can be more informative. Disease stage is determined by computed tomography (CT) scan of the chest and pelvis followed by a confirmational biopsy; and primarily determines outcome [5].

PDAC therapy has evolved over time. For non-resectable disease, the antimetabolite 5-fluouracil was used until 1997 when Buris et al. [38] demonstrated a median survival benefit of another antimetabolite gemcitabine over 5-fluorouracil (5.65 vs 4.41 months, P=0.0025). In 2007, a combination of gemcitabine with erlotinib was shown to further increase survival (6.24 vs 5.1 months, HR = 0.82, 95% CI = 0.69-0.99, P=0.038) [39]. In 2011, the PRODIGE trial [40] demonstrated significantly improved overall survival in patients treated with FOLFIRINOX, a combination of an antimetabolite (5-fluorouracil), DNA damaging agents (oxaliplatin, irinotecan) and leucovorin; vs gemcitabine alone (11.1 vs 6.8 months, HR = 0.57, 95% CI = 0.45-0.74, P<0.001). Quality of life after 6 months was improved in those who received FOLFIRINOX despite having a higher

degree of toxicity [38]. In 2013, the MPACT trial demonstrated that combining gemcitabine with albumin bound paclitaxel further improved overall survival vs gemcitabine monotherapy (8.5 vs 6.7 months, P<0.001) [41]. In 2015, the NAPOLI-1 trial demonstrated improved overall survival by combining nano liposomal irinotecan, fluorouracil and leucovorin compared to fluorouracil and leucovorin (6.1 vs 4.2 months, HR = 0.67, 95% CI = 0.49-0.92, P = 0.012) as a second line treatment [42]. More recently, in 2019 the POLO trial validated germline BRCA1/2 as a genetic biomarker. Eligible patients were prescribed a poly(adenosine diphosphate-ribose) polymerase (PARP) inhibitor, Olaparib, or placebo as maintenance therapy; there was no observed change in overall survival (HR = 0.83, 95% CI = 0.56-1.22, P = 0.35) but progression free survival was improved with maintenance Olaparib after upfront platinum therapy (7.4 vs 3.8 months, HR = 0.53, 95% CI = 0.35-0.82, P=0.004) [43]. The utility of novel treatments such as PD-L1 targeting immunotherapy remains undetermined for PDAC; in 2020, the PA.7 trial by the Canadian cancer trials group investigated if combining immune checkpoint inhibitors such as durvalumab, an anti PD-L1 monoclonal antibody, and tremelimumab, an anti-CTLA-4 antibody, with gemcitabine and nab-paclitaxel would improve treatment efficacy. There was no improvement in overall or progression free survival observed although analysis to identify any potential subgroups that derived benefit remain in progress [44]. The current standard of treatment makes use of systemic therapy with gemcitabine and nab-paclitaxel or FOLFIRINOX for patients with non-resectable PDAC. Given the high degree of toxicity associated with FOLFIRINOX, its application is often limited to younger patients or those with good performance status.

The only curative treatment available is surgical resection followed by adjuvant therapy in patients with resectable PDAC; those with good performance status are given mod-

ified FOLFIRINOX whereas gemcitabine alone or in combination with capecitabine is recommended for those with poor performance status [44]. Recently, the five-year overall survival rate from the PREOPANC trial showed an improved survival (20.5% vs 6.5%) in patients with resectable and borderline resectable tumours when given neoadjuvant gemcitabine based chemoradiotherapy followed by adjuvant gemcitabine vs upfront surgery [45]. Meta-analysis show the possibility of converting locally advanced to resectable tumours, where 10-35% of patients given neoadjuvant either with or without radiotherapy could be downstaged allowing for surgical resection [21, 46]. Radiotherapy is infrequently used for PDAC as the tumours are radioresistant. Its utility is limited to those with locally advanced or borderline unresectable disease. Radiochemotherapy is used where chemotherapy with gemcitabine, capecitabine or 5-FU are given as radio sensitizing agents prior [5]. To date, no metabolically targeting therapy has been approved to treat PDAC. However, one clinical trial (NCT03450018) targeting carbonic anhydrase IX (CA-IX) is currently recruiting patients. CA-IX is a cell surface enzyme that is induced by HIF1α to maintain a tumour favorable PH microenvironment. HIF1α mediates metabolic reprogramming to favor glycolysis and also alter oxidative phosphorylation oxidative phosphorylation (OXPHOS) [47].

1.1.7 *Genomic and Transcriptomic Heterogeneity*

The last two decades have seen major advances and efforts to increase our comprehension of the human genome, including cancer genomes. Analysis have shown high mutation rates in major driver genes in PDAC such as the proto-oncogenic GTPase *KRAS* (>90%), *TP53* (>70%), *CDKN2A* (30%), and *SMAD4* (>30%), amongst other mutations (Figure 1.1) [29]. Darwinian processes generate oncogenic point mutations which aggregate and are selected for by pressures in the tumour microenvironment.

Pathways affected include DNA damage repair, cell cycle regulation, TGB-B signalling and chromatin regulation.

More recently, several next generation sequencing efforts have further uncovered the complex genomic and transcriptomic landscape of PDAC. Many groups have attempted to group individual genes either by molecular mechanism or biological pathway, extending strategies applied in other cancer types to PDAC. Initially, Collison et al. used microdissected epithelium from treatment naive resected tumours and profiled them via global gene expression analysis. Combined with expression data from other human and mouse PDAC cell lines, they classified tumours into three subtypes: classical, QM-PDA and exocrine-like. The QM-PDA subtype corelated with high tumour grade and mesenchyme-associated genes such as *AIM2*, *GPM6B* and *NT5E*; to name a few. In vitro, QM-PDA cell lines displayed greater sensitivity to Gemcitabine than the classical subtype. The classical subtype exhibits KRAS dependency and associates with epithelial genes such as *TMEM45B*, *TFF1* and *MUC13*; as well as the endodermal specifying transcription factor, GATA6. Classical tumours had increased survival compared to with a QM-PDA subtype, post resection. In vitro, unlike QM-PDA cell lines, classical cell lines displayed greater sensitivity to erlotinib. The exocrine-like subtype had a comparatively high expression of digestive enzyme genes. Patient with exocrine-like tumours had the best survival rates. However, this subtype was largely missing in cell line based classifications which could be explained by stromal absence from the microdissection based preparation of tissue samples used for the training cohort [48, 49].

Moffitt et al. built on these subtypes by defining stromal-based classifications using bulk resected, primary untreated PDAC tumours and metastass, which they profiled using hybridization arrays with a subset profiled using RNAseq; excluding any tran-

scripts relating to the normal pancreas. They classified tumours into two primary subtypes which themselves were stratified again by two stroma types; yielding basal-like with normal stroma, basal-like with activated stroma, classical with normal stroma and classical with activated stroma subtypes. The basal-like subtype defined here was consistent with those from other cancers in that it too had high expression of laminins, keratins and genes like *VGLL1*, *UCA1* and *S100A2*; to name a few. These tumours had a significantly higher KRAS G12D mutation rate. Patients with basal-like tumours had the worst overall survival (11 vs 19 months, P=0.007) as well as a lower one year survival rate (44% vs 70%, P=0.007), compared to the classical subtype. The classical subtype had low expression of basal-like genes but high expression of adhesion associated proteins, ribosomal and epithelial genes and genes including *BTNL8*, *FAM3D*, *SMAD4* and *ATAD4*, and similar to Collisson et al.'s classical subtype, increased expression of *GATA6*. These tumours had a significantly higher KRAS G12V mutation rate. All cell lines assayed in the study were classified as basal-like [50, 51]. Amongst the unique stromal subtypes, activated stroma had expression of macrophage associated genes like the integrin *ITGAM*, chemokine ligands *CCL13* and *CCL18*; *SPARC*, wnt members like *WNT2* and *WNT5A*; *MMP9* and *MMP11*. Furthermore, fibroblast activation protein (FAP) was also present in gene signatures for activated stroma. Patients with activated stroma had lower overall survival (15 vs 24 months, P=0.019) and lower one year survival rates (60% vs 82%, P=0.019) compared to those with normal stroma. Normal stroma had higher expression of stellate cell markers like *ACTA2*, *VIM* and *DES*. Interestingly, these stromal subtypes were completely absent from all cell lines and expressed at low levels in many metastatic samples [50, 51].

Bailey et al. profiled treatment naïve primary tumours with stroma included, like Moffitt et al., via whole-genome and deep-exome sequencing, with gene copy number

analysis. A subset of 96 tumours with epithelial content >40% were selected to further undergo RNAseq. They classified tumours into squamous, pancreatic progenitor, immunogenic and aberrantly differentiated endocrine exocrine (ADEX) subtypes. The squamous subtype was characterized by mutations in *TP53* and *KDM6A*, upregulated TP63ΔN transcriptional network, hypermethylation, and downregulation of endodermal cell-fate determining genes such as *GATA6*, *HNF1B*, *MNX1* and *PDX1*. Overall survival was poorest in squamous tumours (13.3 vs 23.7-30 months) compared to all other subtypes. The pancreatic progenitor subtype had high expression of early pancreas development genes such as *PDX1*, *FOXA2/3*, *HNF4A/G* and *MNX1*; fatty acid oxygen regulators, steroid hormone biosynthesis genes, drug metabolism, O-linked glycosylation and mucins such as *MU5AC* and *MUC1*. The ADEX subtype, a subclass of pancreatic progenitor, had high expression of late pancreas development genes like the transcription factors *NR5A2*, *MIST1* and *RBPJL* involved in exocrine differentiation, endocrine differentiation genes (*NEUROD1* and *NKX2-2*) and *MODY*; and genes involved in KRAS activation. The immunogenic subtype had high expression of immune network influencers like B cell signalling pathways, antigen presentation, CD4+ T cell, CD8+ T cell and Toll-like receptor pathways, CTLA4 and PD1 suppression pathways; to name a few. These subtypes were also represented in array-based mRNA expression profiles of tumours not filtered for epithelial content. Overall, the squamous subtype was similar to the previously described QM-PDA and basal-like subtypes, the pancreatic progenitor aligned with the classical subtype and the ADEX subtype was similar to the exocrine-like subtype [50, 52].

Puleo et al. further added to these subtypes by profiling 300 formalin fixed paraffin embedded PDAC tissues excluding transcripts relating to normal pancreas epithelium. They classified tumours into pure basal-like, stroma activated, desmoplastic, pure clas-

sical and immune classical subtypes. The pure classical was defined by a low stromal component; immune classical with a high stromal signature, structural vascularization, immune stroma along with a low proteosome/apoptosis signal; pure basal like too had a low stromal component; stroma activated had a high stromal component defined by increased expression of *α-SMA*, *SPARC*, and *FAP*; and desmoplastic subtype had a basal association, low tumour content, high stromal content inclusive of immune and inflammatory stroma and also had high expression of structural and vascularized stromal components [53]. These subtypes further validated classifications by previous groups.

Taken together, two major molecular subtypes emerge based on endodermal-pancreatic identity, basal-like and classical. There is a strong overlap between squamous/basal-like/QM-PDA subtypes which are associated with poor prognosis; and classical/pancreatic progenitor/ADEX subtypes which have a less worse prognosis (Figure 1.2) [54].

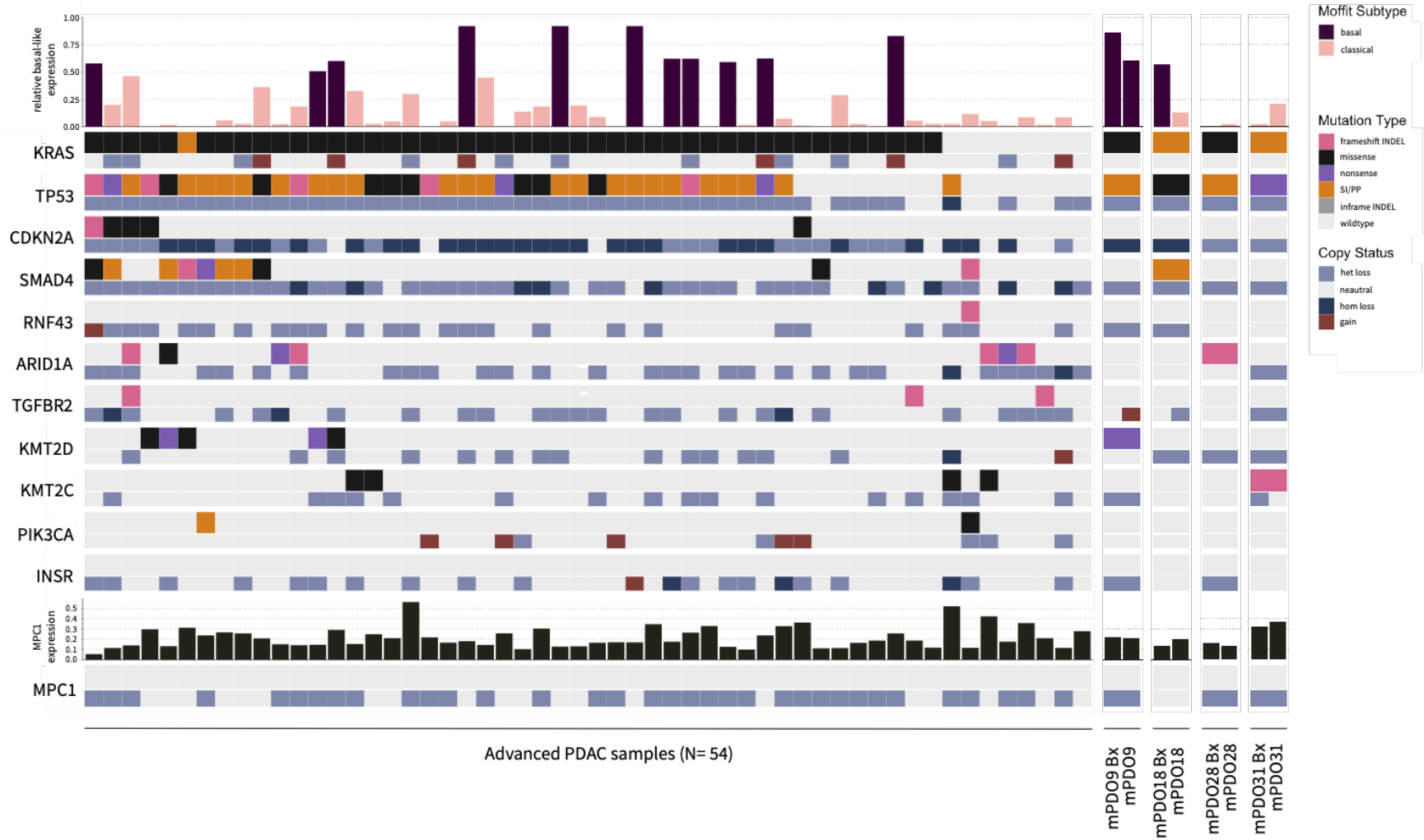
relative basal-like expression
1.00
0.75
0.50
0.25
0.00
KRAS
TP53
CDKN2A
SMAD4
RNF43
ARID1A
TGFBR2
KMT2D
KMT2C
PIK3CA
INSR
MPC1 expression
0.5
0.4
0.3
0.2
0.1
0.0
MPC1
Advanced PDAC samples (N= 54)
mPDO9 Bx
mPDO9
mPDO18 Bx
mPDO18
mPDO28 Bx
mPDO28
mPDO31 Bx
mPDO31
Moffit Subtype
basal
classical
Mutation Type
frameshift INDEL
missense
nonsense
SI/PP
inframe INDEL
wildtype
Copy Status
het loss
neautral
hom loss
gain

Figure 1.1: Oncoprint of commonly mutated genes in PDAC and MPC1 in the PanGen patient cohort (N=58) and associated PDOs (N=4). Mutation and copy number variance (CNV) of top commonly mutated genes and mitochondrial pyruvate carrier 1 (MPC1) are shown with molecular subtypes for a subset of patients from the PANGEN trial.

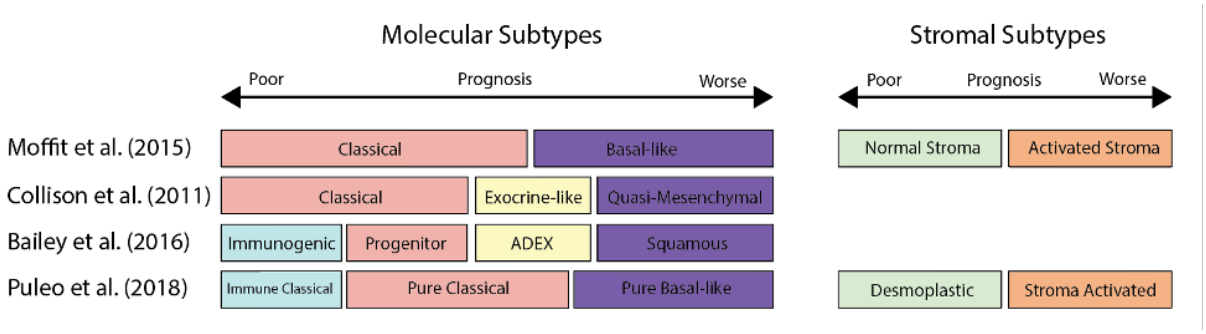

Figure 1.2: Overview of PDAC molecular and stromal subtypes [55, 56].

1.1.8 *Metabolic Heterogeneity*

The heterogeneity in PDAC metabolic alterations gives rise to distinct intertumoral metabolic dependencies. A hallmark of cancer, metabolic reprograming plays a crucial role in oncogenesis and tumour progression. An integrated network of glycolysis, tricarboxylic acid (TCA) and OXPHOS is used by eukaryotic cells to harness energy in the form of ATP and generate downstream metabolites. These pathways begin when glucose enters the cell via the GLUT [57] family and gets converted into pyruvate via glycolysis. If oxygen levels are abundant, this pyruvate either proceeds directly into the mitochondria to participate in the TCA cycle or gets converted to lactate prior to mitochondrial entry via MCT1. This lactate then gets converted to pyruvate inside the mitochondria to participate in the TCA cycle. Intermediates from the TCA cycle force the movement of electrons in the electron transport chain (ETC) and generate a H+ gradient across the inner mitochondrial membrane. These H+ return to the matrix through the ATP synthase F0/F1 complex and are subsequently oxidized, this movement is coupled to the catalysis of ADP to ATP. In tumour cells, however, the rate of glucose uptake and subsequent lactate production is abnormally increased despite ample oxygen availability, a phenomenon known as the Warburg effect [58]. Tumour cells increasingly rely on glycolysis to generate ATP, nucleotide, lipid and amino acid to fuel growth to fuel their rapid growth. Increased proliferation rates along with high stroma and abnormal vascularization create hypoxic conditions. To survive and proliferate under these hostile conditions, tumours have been shown to reprogram intermediary metabolic pathways to favor glycolysis [59]. Concurrently, abnormal oncogene (e.g. *PI3K*, *HIF1A*, *MYC* and *AKT*) and pathway activation further drive the tumour towards utilizing glycolysis for primary energy production, despite normoxic conditions. These altered energy demands reduce the pool of pyruvate entering the

mitochondria to participate in the TCA cycle [58, 60, 61].

Metabolic heterogeneity has become increasingly apparent and several groups have described distinct metabolic subtypes in PDAC. Initially, Daemen et al. utilizing a panel of 256 metabolites in 38 PDAC cell lines classified PDAC into three metabolic subtypes: slow proliferating, glycolytic and lipogenic [49]. Cell lines in the slow proliferating subtype on average had a longer doubling time relative to other two. Though, glycolytic and lipogenic subtypes had differing metabolic profiles. Glycolytic lines had increased levels of glycolytic and serine pathway metabolites including phosphoenolpyruvate, glyceraldehyde-3-phosphate, lactate, and serine. They also have lower levels of OXPHOS products including NAD, NADH, NADP, NADPH, GSSG, GSH, and FAD. Transcription of glycolysis and pentose phosphate pathway genes such as *ENO2* was upregulated. A translational but not transcriptional increase in MCT1 levels was noted as well. Mass spectrometry analysis showed a higher utilization of glutamine than glucose for the TCA cycle in these lines. In vivo, glycolytic tumours appeared aggressive, having high proliferation and metastasis rates, as well as poor response to chemotherapy, relative to lipogenic tumours. Lipogenic lines had increased levels of lipid and OXPHOS metabolites including palmitic acid, oleic acid, palmitoleic acid, myristic acid, coenzyme Q9, coenzyme Q10, aspartate and glutamate. Transcriptionally, lipogenic lines had increased expression of genes involved in cholesterol and de novo lipid synthesis such as *DHCR7*, *SCD*, and *FASN*. Mass spectroscopy of these lines revealed a higher proportion of glucose utilization for the TCA cycle and in lipid metabolites. These subtypes also associated with the previously defined molecular subtypes having a correlation between glycolytic and QM-PDA subtypes; and lipogenic and classical subtypes [49].

In a separate study, Zhao et al. identified six transcriptomic subtypes using a collective of 13 publicly available datasets. These subtypes, L1-6, were individually enriched with genes from several cellular processes. L1 had high expression of carbohydrate genes including *ALDOB*, *CA2*, *NPC1L1* and *PGC*; L2 had high expression of proliferation and epithelial associated including *CCNB2*, *CDKN2A*, *SFN*, *UBE2C*, *SPRR3*, *DHRS9* and *CRABP2*; L3 had high expression of extra-cellular matrix (ECM) related genes such as *GREM1*, *MFAP5*, *COL12A1*, *COL10A1*, *COL8A1*; L4 had high expression of immune related genes including *CCL*, *CCR7* and *CD*; L5 had high expression of neuroendocrine genes including *PAX6*, *IAPP*, *G6PC2*, *ABCC8* and *ZBTB16*; and L6 was enriched for metabolic genes including those of lipid and protein digestive enzymes such as *CLPS*, *PLA2G1B*, *CEL*, *ALB*, *CPA1*, *CPB1*, *CTRL*, *SLC3A1*, *PRSS3* and *ANPEP*. Amongst subtypes with metabolic involvement (L1, L2 and L6), L2 tumours had the worst outcome [62]. A comparison of these with Daemen et al's subtypes revealed similarities between L2 and the glycolytic subtype; while L1 was mixed, having features of both glycolytic and lipogenic subtypes [63].

More recently, our group classified tumours from resectable and advanced PDAC into four metabolic subtypes [64]. These were based on the relative expression of glycolysis and cholesterol-biosynthesis gene sets across a combined cohort of 325 resectable and non-resectable PDAC tumours from five datasets. Mixed tumours had high expression of both glycolysis and cholesterol-biosynthesis sets, glycolytic tumours had high expression of only glycolysis genes, cholesterogenic tumours had high expression of only cholesterogenic genes and quiescent tumours had low expression of both sets. Glycolytic tumours had increased expression of *HIF1A*, *LDHA* and *SLC16A3*; and decreased expression of *PRKAA1*, a catalytic subunit of AMPK. Patients with glycolytic tumours showed the lowest median overall survival. In contrast, cholesterogenic tu-

mours had a relatively longer median overall survival than other subtypes. These tumours had increased expression of sterol synthesis transcriptional activator *SREBF2* and decreased expression of genes such as *AKT2*, *AKT3* and *GLS*. Quiescent tumours were observed to suppress amino acid catabolism, nucleotide metabolism and pentose phosphate pathways. Interestingly, stroma did not influence the stratification of these subtypes. Classification of this cohort using previously described molecular subtyping methods revealed that glycolytic, Moffitt basal-like, Bailey squamous and Collison QM-PDA subtypes showed high overlap. In contrast, cholesterogenic, Moffitt classical, Bailey progenitor and Collison classical subtypes showed overlap. Furthermore, it was noted that expression of glycolytic genes positively correlated with basal-like and negatively with classical gene expression; while expression of cholesterogenic genes correlated negatively with basal-like and positively with classical gene expression. Interestingly, expression of mitochondrial pyruvate carriers 1 and 2 was significantly lower in glycolytic tumours and that mitochondrial pyruvate carrier 2 (MPC2) expression was increased in cholesterogenic tumours. It was also found that MPC1 was the target of heterozygous copy loss in more than 60% of advanced PDAC patients [64].

1.2 Structure and Function of the Mitochondrial Pyruvate Complex

The mitochondrial pyruvate complex (MPC) (150kDa) [65] is part of the SLC54 family of mitochondrial transporters [66] and is highly conserved amongst different species. It is a transporter localized in the inner mitochondrial membrane and mediates transport of pyruvate from glycolysis into the mitochondria to fuel aerobic respiration [67]. MPC1 (12kDa) [43] along with MPC2 (14kDa) [65] are two protomers of the MPC. Pyruvate is transported using a proton symport mechanism thus is driven by the proton gradient across the inner mitochondrial membrane [68]. Pyruvate is crucial for cellular

metabolism, acting as a bridge between glycolysis and OXPHOS [69]. Given that MPC controls pyruvate metabolism and that cancer cells prefer to convert pyruvate to lactate via glycolysis [66], MPC is downregulated in multiple cancer types such as renal and colorectal [66, 70], boosting the Warburg effect. There is high variance in expression between patients in the PanGen cohort, with over 60% of PDAC patients having a heterozygous copy loss. However, no mutations in MPC1 were present (Figure 1.1). Loss of MPC1 or MPC2 results in the degradation of the other leading to impaired mitochondrial pyruvate uptake. In the absence of MPC1, it has been shown that MPC2 can form homodimers, however, these are non-functional. Reduced mitochondrial pyruvate influx has been known to aid in tumour progression and subsequent metastasis [66]. Supressing MPC1 expression in pancreatic cells leads to the formation of a spindle like shape and increase in markers of EMT, features of a mesenchymal phenotype [71]. Loss of MPC1 has also been shown to increase stemness in multiple cancer types such as intestinal, prostate and ovarian [66]; and is associated with reduced response to treatment as shown by Chai et al. who reported poor survival in patients with lower MPC1 expression when treated with temozolomide for glioblastoma [72]. One of the most explored pathways that lead to MPC1 reduction is suppression of peroxisome proliferator-activated receptor gamma coactivator 1-alpha (PGC1α), a regulator of cell metabolism [66]. Increasing PGC1α activity has been shown to reduce proliferation and induce apoptosis [70] and that MPC1 is necessary to achieve these effects [66].

1.3 Patient Derived Organoids as Models for Translational PDAC Research

Patient derived organoids (PDOs) were used as PDAC tumour models. As part of the PanGen Trial, multiple biopsy cores are obtained from a metastatic site and undergo whole genome and transcriptome sequencing. One fresh biopsy core was used to

generate PDOs which were are then propagated to generate a living tumour biobank. Establishing PDOs from these clinically, gnomically and transcriptomically annotated tumours gave us a unique opportunity to select to select PDO models based on individual tumour molecular profiles or clinical characteristics. These PDOs recapitulate donor tumour histopathological and genomic features [Figure 1.1 and A.1] therefore serving as donor tumour avatars.

1.4 Analysis of Bioenergetics

The seahorse XFe96 analyzer was used to measure metabolic flux in the form of extracellular acidification rate (ECAR) and oxygen consumption rate (OCR) as surrogates for glycolysis and OXPHOS, respectively. The basis of these assays is recording effects of interference with these pathways at different time points. During a glycolysis stress test, baseline measurements are taken after PDOs are cultured in glucose/pyruvate free assay medium. Deprived of glucose and pyruvate, any ECAR activity is thought to be due to the conversion of CO_2 from OXPHOS to HCO_3 and H+. Any ECAR activity here is regarded as non-glycolytic so these measures are labeled as non-glycolytic acidification. Glucose is added then to stimulate glycolysis, the resulting lactate by product increases ECAR readouts. Oligomycin, a complex V (ATP-synthase) F0 subunit inhibitor, is added to block ATP production by OXPHOS. To keep up with energy demands, the cell upregulates glycolysis to its maximum capacity (glycolytic capacity). This additional rise in glycolysis is referred to as the cells glycolytic reserve. Finally, 2-DG (2-deoxyglucose) is then added which gets converted to 2-DG-6-phosphate, a competitive inhibitor of phosphoglucoisomerase which reduces readouts to initial non-glycolytic levels, concluding the assay [73].

For the mito stress test, cells are grown in glucose- and pyruvate-controlled assay medium. Baseline OCR measurements are taken at the start. Oligomycin is then added which reduces H+ influx into the mitochondria there by hyperpolarizing the membrane which further prevents flow of H+ through respiratory complexes reducing the rate of respiration. Any respiration still occurring could be due to flow of protons through lipids, mitochondrial damage or other channels. The uncoupler, carbonyl cyanide-4-(trifluoromethoxy) phenylhydrazone (FCCP) is then added which functions as a protonophore. This causes a reversal of the membrane hyperpolarized state drives increases in ETC to maximum levels, highlighting the cells spare respiratory capacity. Antimycin-A and Rotenone, inhibitors of ETC are then added which cause a seizure of all mitochondrial respiration and gives OCR floor value, concluding the assay [73].

1.5 Thesis Rationale, Hypothesis and Aims

Access to sufficient nutrients is limited in PDAC due to extensive desmoplasia and poor perfusion [74]. The majority of PDAC patients have mutations in oncogenes such as KRAS and TP53 (Figure 1.1), with further downstream changes in pathways associated with tumour metabolism and progression [64]. Combined, these conditions drive tumours to undergo metabolic reprogramming. Aspects of this reprogramming include elevation of glycolysis through the Warburg effect. Recent efforts have elucidated several transcriptome-based metabolic subtypes. It was shown that MPC1 is a target of heterozygous copy loss in over 60% of metastatic PDAC patients. Tumours from these patients with a glycolytic subtype had the lowest levels of MPC1 and MPC2, suggesting reduced transport of pyruvate into the mitochondria. Furthermore, tissue microarray data of resected PDAC showed reduced MPC1 protein expression in short term survivors (OS = 6-12 months). Therefore, we hypothesized that individual PDAC

tumours have different levels of glycolysis and oxidative phosphorylation and that targeting MPC1 will alter tumour metabolic profiles. My specific aims are:

Aim 1: Adapt a cellular metabolic assay and develop a protocol to analyze glycolysis and oxidative phosphorylation specifically in three-dimensional tumour organoid models

Aim 2: Investigate the levels of glycolysis and oxidative phosphorylation in tumour organoids derived from individual tumour biopsies

Aim 3: Investigate the effect of agents targeting MPC1 and tumour metabolism on glycolysis and oxidative phosphorylation in tumour organoid models.

Chapter 2: Methods

2.1 Establishing and Propagating Patient Derived Organoid Lines

A fine needle biopsy sample was obtained from metastatic lesions in patients enrolled via the PanGen trial (NCT02869802). Tissues were dissected such that any necrotic regions and blood vessels were excised followed by addition of digestion media (5mg/mL Collagenase II (Thermo Fisher, 17101015) in complete growth media (CGM)). The suspended tissue was then minced and placed at 37ºC for 12-16 hours. Digestion media was removed, cells were suspended in Matrigel domes and grown in CGM (advanced DMEM/F12 (Thermo Fisher, 12634010), GlutaMAX 1X (Thermo Fisher, 35050061), HEPES 10mM (Thermo Fisher, 15630080), Primocin 100ug/mL (Invivogen, ant-pm-1), B-27 Supplement 1X (Thermo Fisher, 17504044), N-Acetyl-L cysteine 1.25mM (Sigma, A9165), Gastrin-I (I-14) 10nM (Sigma, G9020), Recombinant Human FGF-10 100ng/mL (Peprotech, 100-26), A 83-01 0.5 μM (Tocris, 2939), Y-27632 10 μM (Tocris, 1254), Nicotinamide 10 μM (Sigma, N0636), Recombinant Human EGF 50ng/mL (AF-100) and Wnt-3a/R-spondin1/Noggin conditioned medium v/v 50% (ATCC, CRL-3276). Organoids grown from these samples are referred to as PDOs.

PDOs were grown at 37ºC in 5% CO_2 with recurring 4-day media changes and were passaged upon reaching 80-90% confluency. To passage, media was aspirated and 1mL 1X TrypLE Express (Thermo Fisher, 12604013) was added to the well. Cells were then suspended in TrypLE and the plate was incubated at 37ºC 5% CO_2 with cells being resuspended at 10 min intervals. Adv DMEM/F12 then added in a 2:1 ratio and contents of well were transferred to a falcon tube. Cells were then counted using

a haemocytometer and an appropriate volume was aliquoted. The aliquot was then centrifuged at 300 RCF and the pellet was resuspended into Matrigel domes followed by addition of Complete Growth Medium. All cells were grown at 37ºC in 5% CO_2. PDOs were considered established upon reaching a fifth passage with at least a million cells.

2.2 Whole Genome and Transcriptome Sequencing

PanGen and POG samples were subjected to whole genome and transcriptomic sequencing as previously described [64, 75]. Fresh tumour biopsies and matched normal (blood) were sequenced at a target depth of 80X and 40X, respectively. Libraries had reads trimmed to 75 base pairs (bp) and were aligned (hg19; GRCh37-lite) using BWA-mem v0.7.6a [76] with default parameters and duplicate reads were marked using sambamba v0.5.5 [77] with default parameters. RNA sequencing had a target depth of 200 million reads and reads were trimmed to 75bp and aligned (GRCh37-lite) using STAR v2.7.3 [78] with parameters: -chimSegmentMin 20 -outSAMmultNmax 1 -outSAMstrandField intronMotif -outFilterIntronMotifs RemoveNoncanonical; and duplicate read were marked using PicardTools v2.17.3. Raw reads counts were assigned to Ensembl 75 genes using Subread v1.4.6 [79], normalized for library depth and gene size (RPKM) and log10-transformed. All sequencing was performed at the Canada's Michael Smith Sciences Center at BC Cancer by the Personalized OncoGenomics team.

2.3 Adapting the Seahorse XFe96 Microplate to Patient Derived Organoids and Cell Density Optimization

Assay parameters for utilizing the Agilent 96-well microplates were modified for PDOs. Plates were coated in 30 μL of a 1:10 Matrigel to CGM mix and incubated at room

temperature for 1.5 hrs. To optimize seeding density, the appropriate cell density was added into wells as a 150μL CGM solution. The plate was then placed in a 37^{o}C and 5% CO_2 IncuCyte analyzer for 7 days.

2.4 Measurement of Extracellular Acidification Rates

A glycolytic stress test using the seahorse XFe96 analyzer was used to measure glycolytic parameters in PDOs. Each well of a seahorse 96 well microplate was covered in 30μL of a 1:10 dilution of Matrigel to CGM. The plate was incubated at room temperature for 1.5 hours after which cells were seeded at a density of $1x10^4$. To measure the effects of metabolic agents, cells were incubated for 96 hrs in CGM. Cells were then exposed to the drug of interest for another 48 hours prior to the assay after which the compound was added and the cells were incubated for another 48hrs. 60 mins prior to ECAR measurement, PDOs were washed twice with minute intervals using Glycolysis Assay Medium (Minimal DMEM containing HEPES and no phenol red, 1X Glutamax). Fresh Assay medium was then added to each well and the plate was incubated at 37^{o}C under atmospheric CO_2 levels. Confluency measurements were taken during using an IncuCyte analyzer. Extracellular acidification rate (ECAR) was analyzed was analyzed under basal conditions and after sequential injection of glucose (10 mM), oligomycin (5 mM) and 2-DG (25 mM), three sequential measurements were taken under each new condition All metabolic measurements were normalized to well confluency.

2.5 Measurement of Oxygen Consumption Rates

A mito stress test using the seahorse XFe96 analyzer was used to measure oxygen consumption rates. Each well of a seahorse 96 well microplate was covered in 30 μL

of a 1:10 dilution of Matrigel to CGM. The plate was incubated at room temperature for 1.5 hours after which cells were seeded at a density of $1x10^4$. To measure the effects of metabolic agents, cells were incubated for 96 hrs in CGM. Cells were then exposed to the drug of interest for another 48 hours prior to the assay after which the compound was added and the cells were incubated for another 48hrs. 60 mins prior to oxygen consumption measurement, PDOs were washed twice with one-minute intervals using Mito Assay Medium (Minimal DMEM containing HEPES and no phenol red, 1X Glutamax, 1mM pyruvate). Fresh Assay medium was then added to each well and the plate was incubated at 37°C under atmospheric CO_2 levels. Confluency measurements were taken during using an IncuCyte analyzer. OCR was analyzed under basal conditions and after sequential injections of oligomycin (5 μM), FCCP (2μM) and Rotenone/Antimycin-A (0.5 μM), three sequential measurements were taken under each new condition. All metabolic measurements were normalized to well confluency as described below.

2.6 Cell Viability to Measure Drug Dose

96 well black/clear bottom microplates (Greiner, 655096) were coated with 30μL diluted Matrigel solution (1:10 Matrigel to CGM) and the plate was incubated for 1.5 hrs at room temperature. PDOs were seeded at a density of 5×10^3 cells per well in an additional 70 μL CGM and incubated at 37°C in 5% CO_2 for 96 hrs. PDOs were then exposed to 100 μL of 0-1mM of serially diluted drug in triplicates and incubated for another 72hrs at 37°C in 5% CO_2. The concentration of vehicle control used equated proportionally to the highest volume of drug added. Viability was assessed by adding 21 μL of staining solution (Adv. DMEM/F12, ethidium homodimer 19 μL/mL (Thermo Fisher, E1169), Hoechst 33342 12 μL/mL (Thermo Fisher, H3570) to each well and incubating the plate

for 60 mins. The IN Cell Analyzer 2200 (GE Healthcare) with its companion workstation (v3.7.3) software were then used to capture and analyze 9 fields distributed uniformly per well under both UV and Cy3 channels to count the live and dead cell population. All wells were normalized to the vehicle control.

2.7 Measurement of Confluence

PDOs were seeded in 96 well culture plates and treated, as previously described. The plate was transferred to an IncuCyte ZOOM imaging system and each well was imaged using phase contrast. Images were taken every 4 hours for a definite time period. The companion software was used to train a model using images from current and previous experiments. Using the images and model, cell surface area coverage was quantified as confluence at a single z-plane determined by the device for each well. All experiments were performed in duplicates.

2.8 Statistical Analysis

Seahorse data was processed with a modified version of the SeaHORse Explorer (SHORE) [67] tool. All line and bar graphs were generated using GraphPad Prism (v8.0, San Diego California). Scatter plots were generated within R v4.1.2 in RStudio v1.3. All analysis of ECAR and OCR values including ratios were performed using an unpaired Student's t-test. All correlations were performed as Pearson correlations.

Chapter 3: Results

3.1 Glycolytic and Mitochondrial Extracellular Flux Analysis of PDAC Patient Derived Tumour Organoids

Given the high degree of molecular and metabolic intertumoral heterogeneity in PDAC, we set out to profile the bioenergetics of these tumours. The seahorse XFe96 analyzer [80] was used for all metabolic measurements. The seahorse XFe96 system measures the ECAR and OCR as a function of time. Changes in ECAR and OCR are measured in response to various metabolic inhibitors and substrates, bioenergetic parameters are then calculated. To capture the molecular and metabolic heterogeneity of metastatic PDAC, we used metastatic Patient derived organoid (mPDO) models derived from eight consented patients. However, the seahorse platform was developed for use with two dimension (2D) cell cultures and had to be adapted for use with PDOs. PDOs grow in three dimensions in an ECM and as such perfusion rates are affected when allometric rules such as Kleiber's Law [81] and the ECM are factored in. Therefore, PDOs require a higher concentration of compounds than 2D cultured cells [82]. We set out to optimize protocols for growing, adjusting media compositions and concentrations of metabolic compounds; and normalization methods for PDOs.

3.1.1 *Optimizing Seahorse XFe96 Cell Culture Microplates for PDO Growth and Bioenergetic Measurements*

In contrast to a standard 96 well flat bottom microplate, the seahorse microplate has a two-stage beveled interior where the well diameter at the top is 8.1mm which decreases to 3.81mm at the bottom. The seahorse microplate wells have a height of

15.49mm, there are three equidistant prongs rising from the base with heights of 0.89mm. These prongs function as mechanical pillars for assay cartridge sensors to rest upon, therefore, any organoid/ECM layer is limited to a height of 0.89mm to ensure max compatibility and not hinder sensors. Excluding space occupied by pillars, this gives us a theoretical maximum working volume of 2.29mm^3 (Figure 3.1)[83].

Matrigel diluted in growth media was used to coat each well. The diluted Matrigel solution effectively covered each well with 3μl of Matrigel. Since the density of Matrigel (8-11mg/mL) exceeds that of media (1mg/mL) [84, 85], 1.5 hrs proved to be sufficient for an adequate base layer to form. Assuming all the Matrigel sediments, the height of this layer was calculated as 0.29mm, well below the working height limit. This difference of 0.5mm allows for organoids to be partially exposed as per the Muthuswamy organoid growth technique [86] and provide an adequate buffer zone for metabolites to equilibrate with media for reliable measurement.

3.1.2 *Optimizing PDO Seeding Density*

Given the total time for the assay of 6 days with days 1-4 allocated for organoid formation, it is crucial to have an optimal seeding density which allows organoid formation and continued exponential growth within the defined time parameter, especially prior to treatment. In our analysis of two PDO lines (mPDOs 9 & 18) for growth using an IncuCyte growth assay, it was observed that seeding 1x10^4 single cells initially over 5x10^3 resulted in a ~5 fold increase (Figure 3.1a, c and e) in confluence in mPDO9 and a ~3 fold increase (Figure 3.1b, d and f) in mPDO18 at day 6. Relative growth on day 4 was also significantly higher with 1x10^4 cells and it appeared that this group entered the exponential growth phase earlier in both PDO lines (Figure 3.1a and b). Given this

we proceeded with $1x10^4$ cells as our initial seeding density for all further analyses.

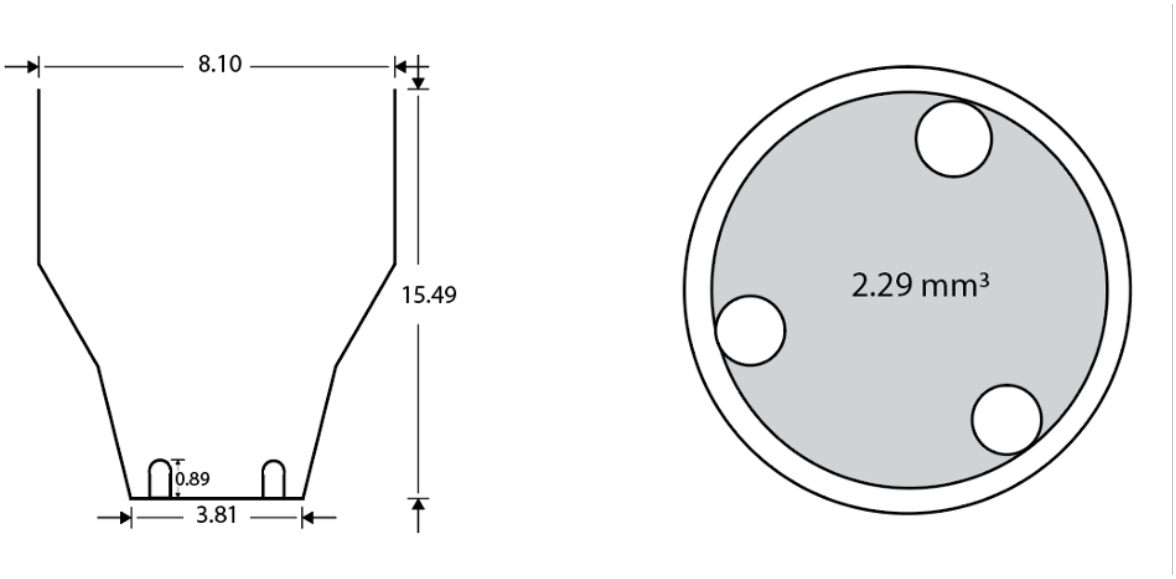

Figure 3.1: Seahorse XFe96 microplate well layout. Seahorse microplate wells have a two stage beveled interior with three prongs at the base. All measurements are in millimeters (mm).

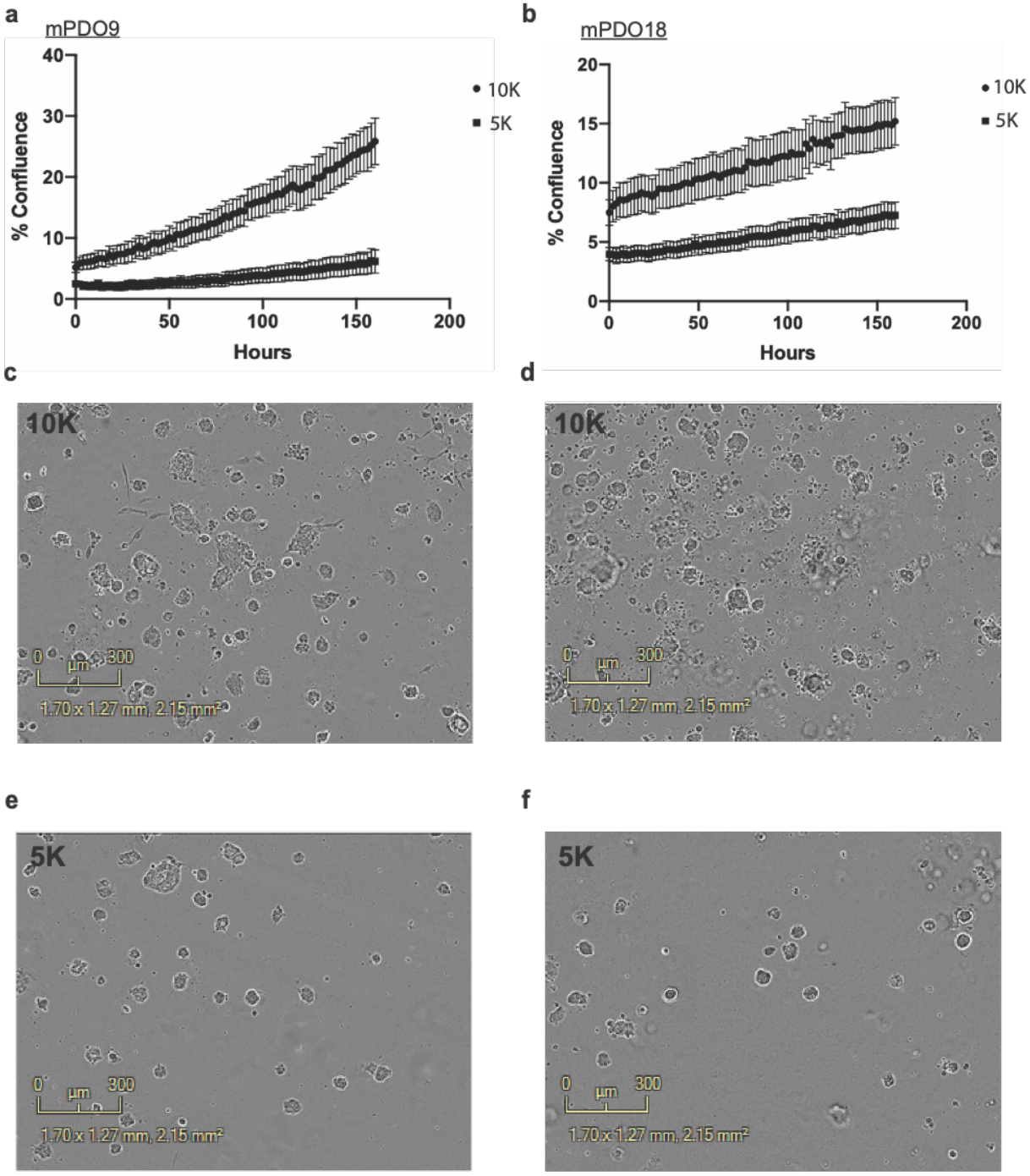
a
mPDO9
% Confluence
Hours
10K
5K
b
mPDO18
% Confluence
Hours
10K
5K
c
10K
0 µm 300
1.70 x 1.27 mm, 2.15 mm²
d
10K
0 µm 300
1.70 x 1.27 mm, 2.15 mm²
e
5K
0 µm 300
1.70 x 1.27 mm, 2.15 mm²
f
5K
0 µm 300
1.70 x 1.27 mm, 2.15 mm²

Figure 3.2: Variability in growth rates by PDO seeding density (a-b) A comparison of seeding 10,000 vs 5000 PDOs at day 0. Images were taken every 4 hours using an IncuCyte ZOOM analyzer and confluency was determined using phase contrast trained model (c-d) Phase contrast images of a sample well on day 6 with $1x10^4$ cells seeded initially (e-f) Phase contrast images of a sample well on day 6 with $5x10^3$ cells seeded initially.

3.1.3 *Optimizing Oligomycin Concentration Used in Assays with PDOs*

Oligomycins are a group of macrolides from streptomyces. Oligomycin A has long been recognized as a potent inhibitor of mitochondrial ATP synthase; it binds to subunit c (rotor ring) of the F0 subunit which serves to catalyze ADP to ATP [87]. Oligomycin is utilized in both the glycolytic stress test and mito stress test. The oligomycin supplied with assay kits is a mixture of oligomycin A, B and C with a >60% Oligomycin A proportion and unknown relative amounts of B and C. Due to limited quantity supplied with assay kits, we utilized externally sourced oligomycin (Sigma Aldrich, O4876) which too was a mixture of oligomycin A (>60%), B and C. We noticed a discordance between results when externally sourced oligomycin was used over vendor supplied, therefore, reduced the number of assay wells to allow use of kit oligomycin.

Using pre-optimized conditions we performed a glycolytic stress test (Figure 3.3a) with 0, 2.5, 5 and 10 μM oligomycin with mPDOs 18 and 42. For reference, 1 μM oligomycin is utilized for 2D PDAC cell lines by our group. There was no difference observed between 2.5-10 μM oligomycin treatments (Figure 3.3b). A similar outcome was observed in mPDO42 except for a slightly higher but not statistically significant, basal glycolysis and glycolytic capacity rate with 10 μM oligomycin (Figure 3.3c). Given these results we proceeded with 5 μM oligomycin for all further analysis.

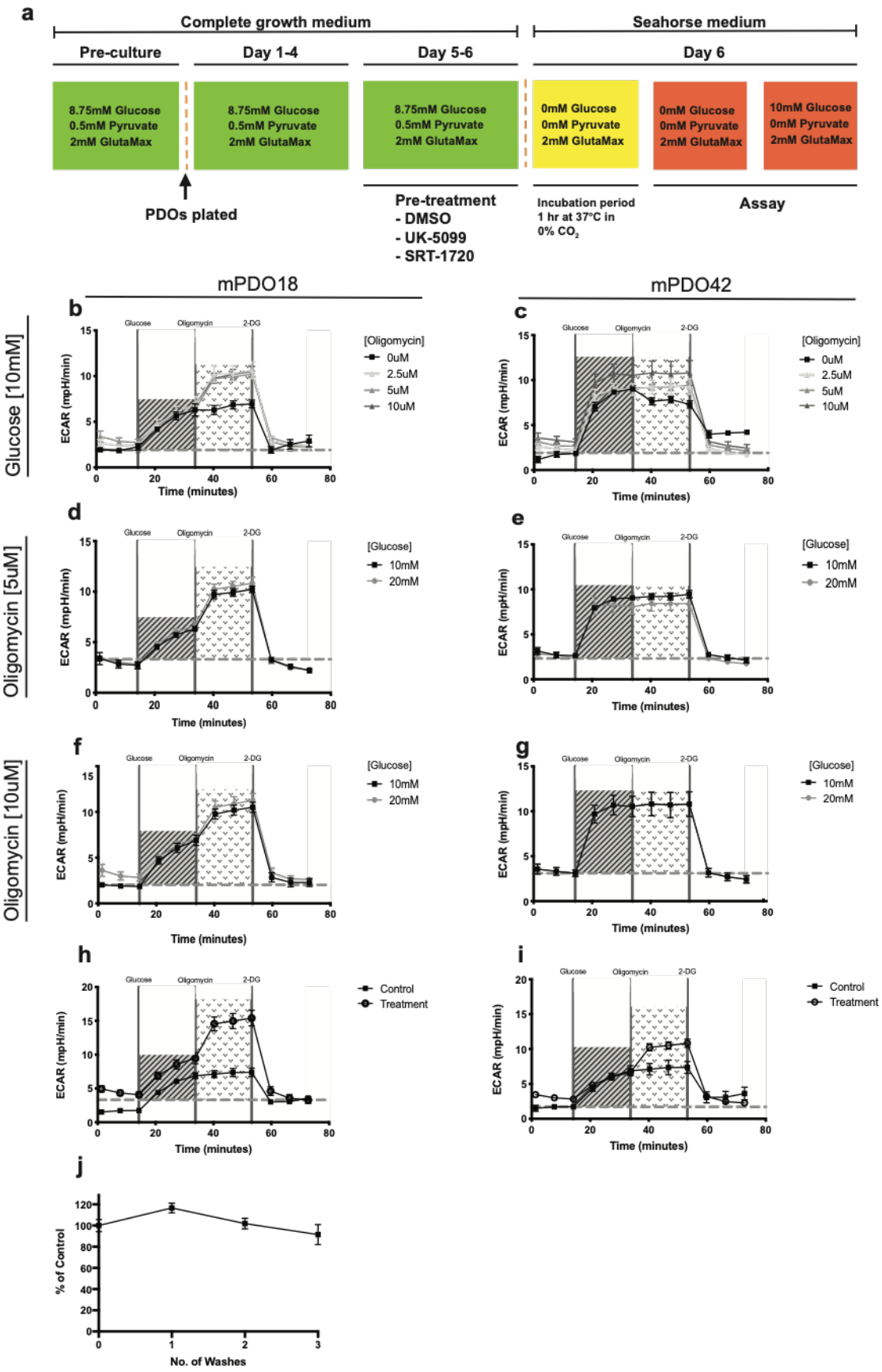
a
Complete growth medium
Seahorse medium
Pre-culture
Day 1-4
Day 5-6
Day 6
8.75mM Glucose
0.5mM Pyruvate
2mM GlutaMax
0mM Glucose
0mM Pyruvate
2mM GlutaMax
10mM Glucose
0mM Pyruvate
2mM GlutaMax
PDOs plated
Pre-treatment
- DMSO
- UK-5099
- SRT-1720
Incubation period
1 hr at 37°C in
0% CO2
Assay
mPDO18
mPDO42
Glucose [10mM]
Oligomycin [5uM]
Oligomycin [10uM]
b
c
d
e
f
g
h
i
j
Glucose
Oligomycin
2-DG
ECAR (mpH/min)
Time (minutes)
[Oligomycin]
0uM
2.5uM
5uM
10uM
[Glucose]
10mM
20mM
Control
Treatment
% of Control
No. of Washes

Figure 3.3: Optimization of Seahorse XFe96 glycolysis stress assay for utility on PDO research. (a) Timeline of glycolysis stress assay and changes in media composition. (b) Increased oligomycin concentrations show no difference in glycolytic measures (ECAR, mean ± SEM) in mPDO18 and (c) mPDO42. (d) Injecting 20mM over 10mM glucose does not increase glycolytic rates when used with 5 μM oligomycin in mPDO18 and (e) mPDO42 (f). Injecting 20mM over 10mM glucose does not increase glycolytic rates when used with 10 μM oligomycin in mPDO18 and (g) mPDO42 (h). High variability in raw data is reduced when (i) normalized by PDO confluency (j) Wash count of PDOs showing no significant reduction in PDO count between 1-3 washes.

3.1.4 *Optimizing Glucose Concentrations Used in Assays with PDOs*

PDOs are cultured in CGM which at minimum has 157.5 mg/dL (~8.75mM) glucose present. In comparison, 2D PDAC cells are typically cultured in high glucose DMEM (10% FBS) containing 450mg/dL (25mM) glucose. Given that physiological glucose lies between 80-90 mg/dL and rises to 120-140 mg/dL postprandially [88], PDOs are grown in slightly higher glucose than physiologically occurring but significantly less than that used for 2D cell culture and levels occurring in those with diabetes (200mg/dL) [89]. PDOs/cells are cultured in glucose deprived medium during a glycolytic stress test (Figure 3.3a). Since 10mM glucose is used when assaying 2D cells, we were curious if PDOs would require a higher concentration of glucose to achieve a similar boost in glycolysis after injection. Glycolysis stress tests were performed on mPDOs 18 and 42 where 10 or 20mM glucose injections were used in conjunction with either 5 μM (Figure 3.3d and e) or 10 μM (Figure 3.3f and g) oligomycin. In all combinations, there was no observed advantage of using 20mM glucose.

3.1.5 *Optimizing Wash Count to Minimize Detachment of PDOs*

Prior to start of assay, CGM has to be replaced with assay media to allow for reliable bioenergetic measurements. Two washes are the standard for assays with 2D cell lines. Given that PDOs lie atop a Matrigel layer, this creates the risk of them becoming dislodged with excessive force. Furthermore, the rate of diffusion is lowered as media travels through Matrigel pores. In order to minimize PDO loss while effectively replacing all media, PDO wells were washed either 0, 1, 2 or 3 times with a one-minute interval between every wash. A staining solution composed of 12μL/mL Hoechst, a total nuclear stain, and ~19μL/mL ethidium bromide, a stain for dead or dying cells,

was added to each well, the plate was incubated at 37°C in 5% CO_2 for 1 hour and scanned using the IN Cell Analyzer 2200 platform. The seahorse plate was found to be not fully compatible with the IN Cell Analyzer but one field at the center of the well was obtained. There was no significant difference observed between wash counts (Figure 3.3j). Hence, we decided to proceed with the standard two washes with the added one- minute interval to ensure complete media exchange.

3.1.6 *Identifying and Optimizing a Normalization Methodology for PDOs*

A crucial step in the analysis of ECAR and OCR values is the normalization of cell number data between control and treatments, to ensure reliable comparison. Commonly used approaches include total DNA, total protein and imaging-based methods. Since PDOs are grown on a Matrigel matrix bed, total protein levels would be contaminated by protein content from Matrigel. Due to the high throughput design of the microplate including relatively low cell numbers in comparison to a 6/12 well plate or T175 flask, adequate DNA quality controls cannot be achieved, thus this method proved difficult to adapt. We proceeded to utilize an imaging-based approach. PDOs were grown and treated as defined previously. An IncuCyte zoom imaging system was used to capture phase contrast images of each well after washes but prior to seahorse analysis. Using a multi-image PDO trained confluency analysis model we were able to quantify PDO coverage on a single z-plane. Plotting of non-normalized data shows variance in glycolysis beyond that which can be attributed to non-glycolytic acidification (Figure 3.3h) indicating differences could be attributed to differences in cell number. Confluency percentages when used to normalize all ECAR and OCR values reduced curve variance to non-significance (Figure 3.3i).

3.2 Exploring the Time-Dose Relationship in Metabolic Effects of SRT-1720

We analyzed viability in PDOs treated with SRT-1720, a sirtuin 1 (SIRT1) activator which leads to the activation of PGC1α. PDOs were treated with SRT-1720 for 48hrs. A dose range of 0.05-100 μM was tested in mPDOs 31 and 18 (Figure 3.4a). In mPDO31, treatment with SRT-1720 had no significant effect up to a dose of 0.1mM, after which a higher overall cell count was noted for doses 0.5-5 μM (Figure 3.4b) which is a known phenomenon occurring due to heat distribution limitations in 96 well plates. There was noticeable cell death at 10 μM indicating the onset of cytotoxicity occurs higher than 5 μM and lower than 10 μM, with the EC50 being 10.92 μM (Figure 3.4a) and complete cell death was noted for does exceeding 10 μM. Interestingly, a nearly identical effect was observed for mPDO18 (Figure 3.4c) as well with the EC50 values also at 10.92 μM (Figure 3.4a). In our efforts to treat PDOs with the maximal tolerable dose, supported by these results, 5 μM was selected as the optimal candidate dose for metabolic testing.

We proceeded to revaluate the tolerable dose with an increased treatment time of 72 hours. The two mPDO lines treated were mPDO9 and 18. Interestingly, an extra 24 hours of treatment reduced EC50 values by more than half to 4.56 μM in mPDO18 (Figure 3.4a). There was no effect up to 2.5 μM, after which viability was reduced by at least 50% for all remaining doses (Figure 3.4d). The effect was much more potent in mPDO9 with an EC50 of 2.19 μM (Figure 3.4a). There was no effect observed for doses up to 1 μM after which viability was reduced by at least two thirds in all remaining doses (Figure 3.4e). Overall, there was a leftward shift in EC50 curves. Due to the increased toxicity at 72 hours between PDOs, treatment time was limited to 48 hours in metabolic experiments.

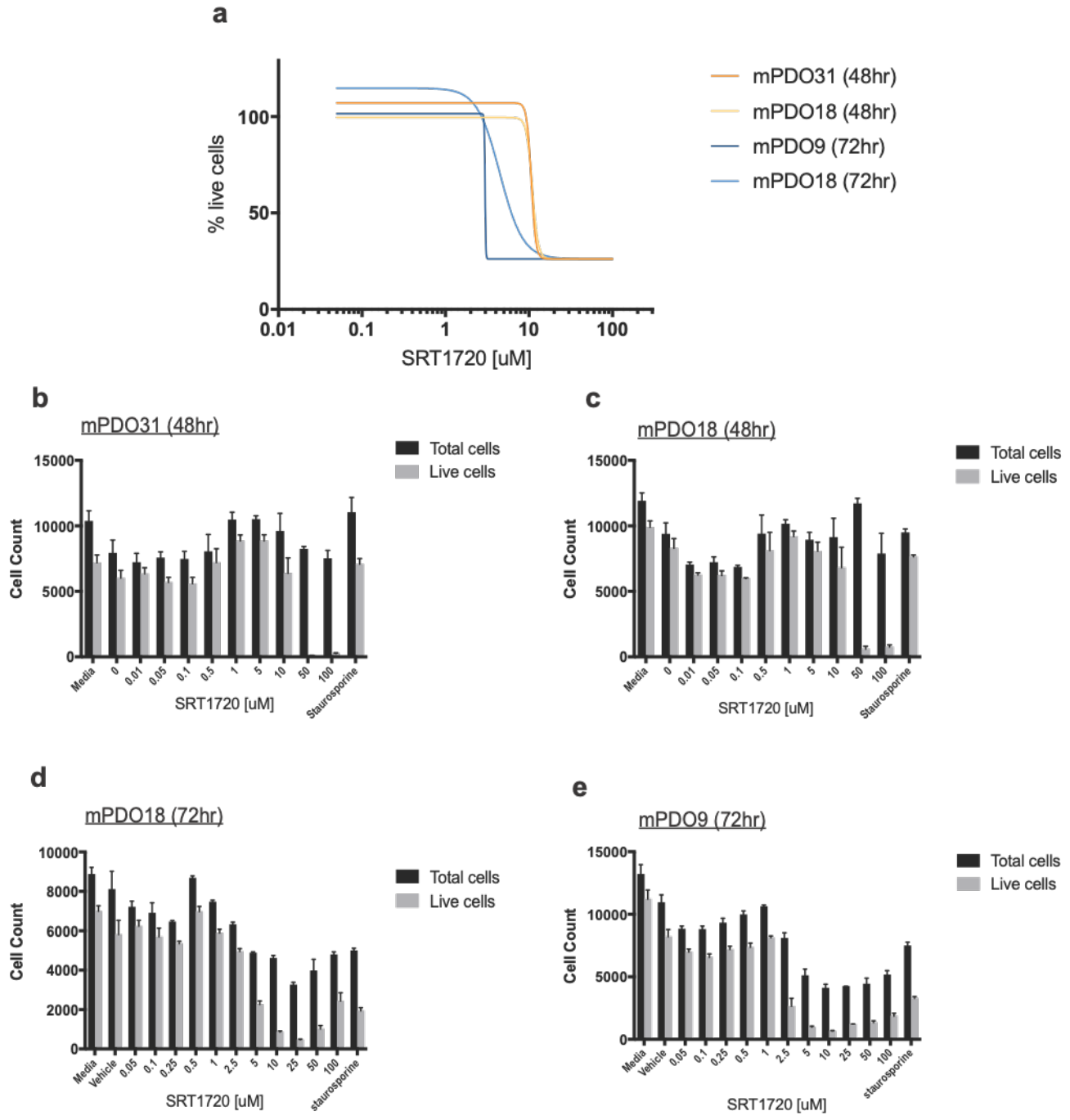
a
% live cells
100
50
0
0.01
0.1
1
10
100
SRT1720 [uM]
mPDO31 (48hr)
mPDO18 (48hr)
mPDO9 (72hr)
mPDO18 (72hr)
b
mPDO31 (48hr)
Cell Count
15000
10000
5000
0
Media
0
0.01
0.05
0.1
0.5
1
5
10
50
100
Staurosporine
SRT1720 [uM]
Total cells
Live cells
c
mPDO18 (48hr)
Cell Count
15000
10000
5000
0
Media
0
0.01
0.05
0.1
0.5
1
5
10
50
100
Staurosporine
SRT1720 [uM]
Total cells
Live cells
d
mPDO18 (72hr)
Cell Count
10000
8000
6000
4000
2000
0
Media
Vehicle
0.05
0.1
0.25
0.5
1
2.5
5
10
25
50
100
staurosporine
SRT1720 [uM]
Total cells
Live cells
e
mPDO9 (72hr)
Cell Count
15000
10000
5000
0
Media
Vehicle
0.05
0.1
0.25
0.5
1
2.5
5
10
25
50
100
staurosporine
SRT1720 [uM]
Total cells
Live cells

Figure 3.4: Assessment of SRT-1720 toxicity in PDOs. (a) Viability curves of mPDOs 31 (EC50 = 10.92 μM) & 18 (EC50 = 10.92 μM) treated for 48hrs and mPDOs 18 (EC50 = 4.56 μM) & 9 (EC50 = 2.19 μM) treated with SRT-1720 show a leftward shift of EC50 when treatment time is increased by 24hrs. (b) bar graph with cell counts (mean ± SEM) of mPDO31 treated for 48hrs shows cytotoxicity occurs after 5 μM of SRT-1720 (c) bar graph with cell counts mPDO18 treated for 48hrs shows cytotoxicity occurs after 5 μM of SRT-1720 (d) bar graph with cell counts of mPDO18 treated for 72hrs shows cytotoxicity occurs after 2.5 μM of SRT-1720 (e) bar graph with cell counts of mPDO9 treated for 72hrs shows cytotoxicity occurs after 1 μM of SRT-1720.

3.3 Exploring the Metabolic Landscape of PDOs

Since Otto Warburg described the Warburg effect [58], there has been accumulating evidence suggesting the occurrence of metabolic reprogramming in cancer cells. To further investigate, we performed glycolytic stress tests and mito stress tests using a Seahorse XFe96 analyzer. PDOs chosen for this represented a full spectrum of molecular and metabolic subtypes. Based on Moffitt based classifications of their biopsies, the cohort consisted of three basal and five classical PDOs (Figure 3.5). CNV status of key pathway genes differed amongst PDOs; 7/8 had a heterozygous loss of MPC1, 2/8 had a heterozygous loss of PGC1α and 1/8 had a heterozygous loss of MPC2. Baseline glycolytic measurements of PDOs were performed. There was remarkable variation in glycolytic reserves observed amongst all PDOs (Figure 3.6a-h). mPDO9, mPDO18 and mPDO53 had highest reserves equal to more than 50% of their baseline glycolysis levels, followed by mPDO28 with 26%, mPDO45 with 32% reserve, and no glycolytic reserve under the experimental conditions in mPDO31, mPDO42 and mPDO46 (Table 3.1). Baseline respiratory measurements were then performed using the mito stress test (Figure 3.7a). mPDO18, mPDO31, mPDO46 and mPDO53 had spare respiratory capacities equaling to at least 50% of their maximal respiration rates whilst mPDO28 and mPDO45 had reserves of less than 25% (Figure 3.7b-i). mPDO9 had virtually no reserves present (Table 3.2). Interestingly, when the averages of glycolytic reserves as proportions of glycolytic capacities were plotted against Moffitt subtype scores (Figure 1.1 and A.1), we observed a strong positive correlation (R=0.86, P=0.0067) (Figure 3.8) indicating that an increase in a tumours glycolytic bandwidth also increases propensity of basal-like gene expression. Furthermore, there was high glycolysis pathway gene expression in biopsies from which these high reserve PDOs were derived; particularly expression of TPI, GAPDH and HK1 was exceptionally high (Figure 3.5). Overall, we observed

different levels in glycolytic and respiratory capacities between PDO lines derived from different patient tumours, highlighting the potential metabolic heterogeneity between individual tumours.

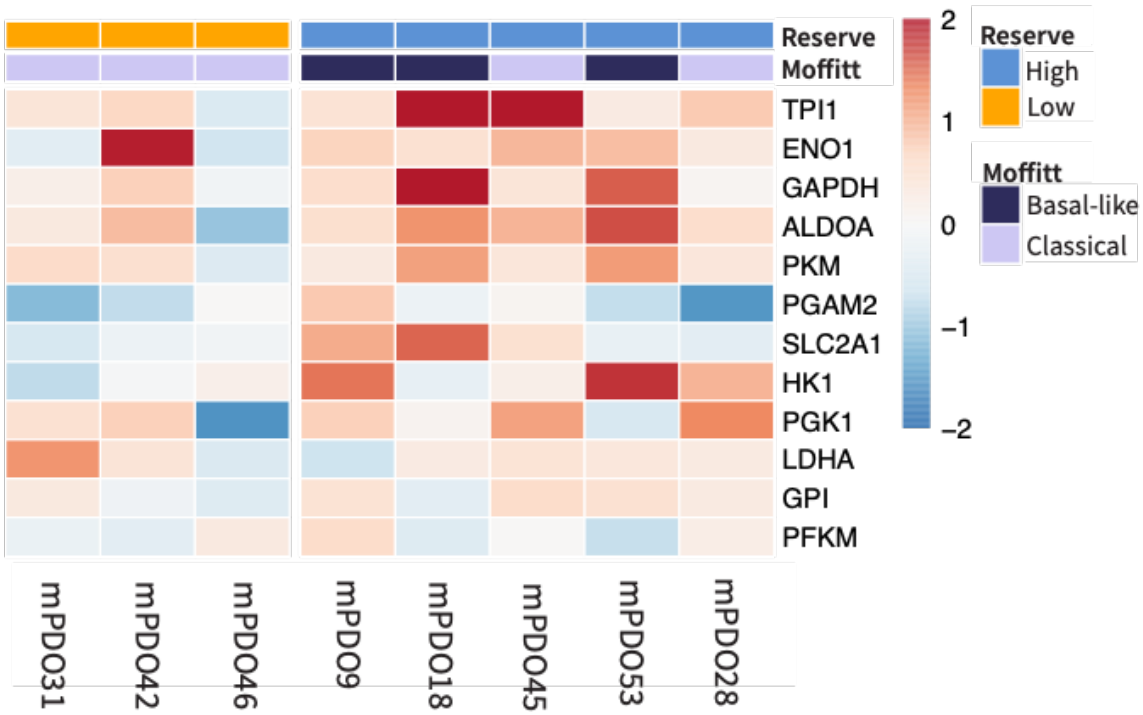

Figure 3.5: Heatmap of glycolysis pathways genes. Overall expression of main glycolytic pathway genes is higher in biopsies from which derived PDOs had a high glycolytic reserve (GR:GC > 0.1).

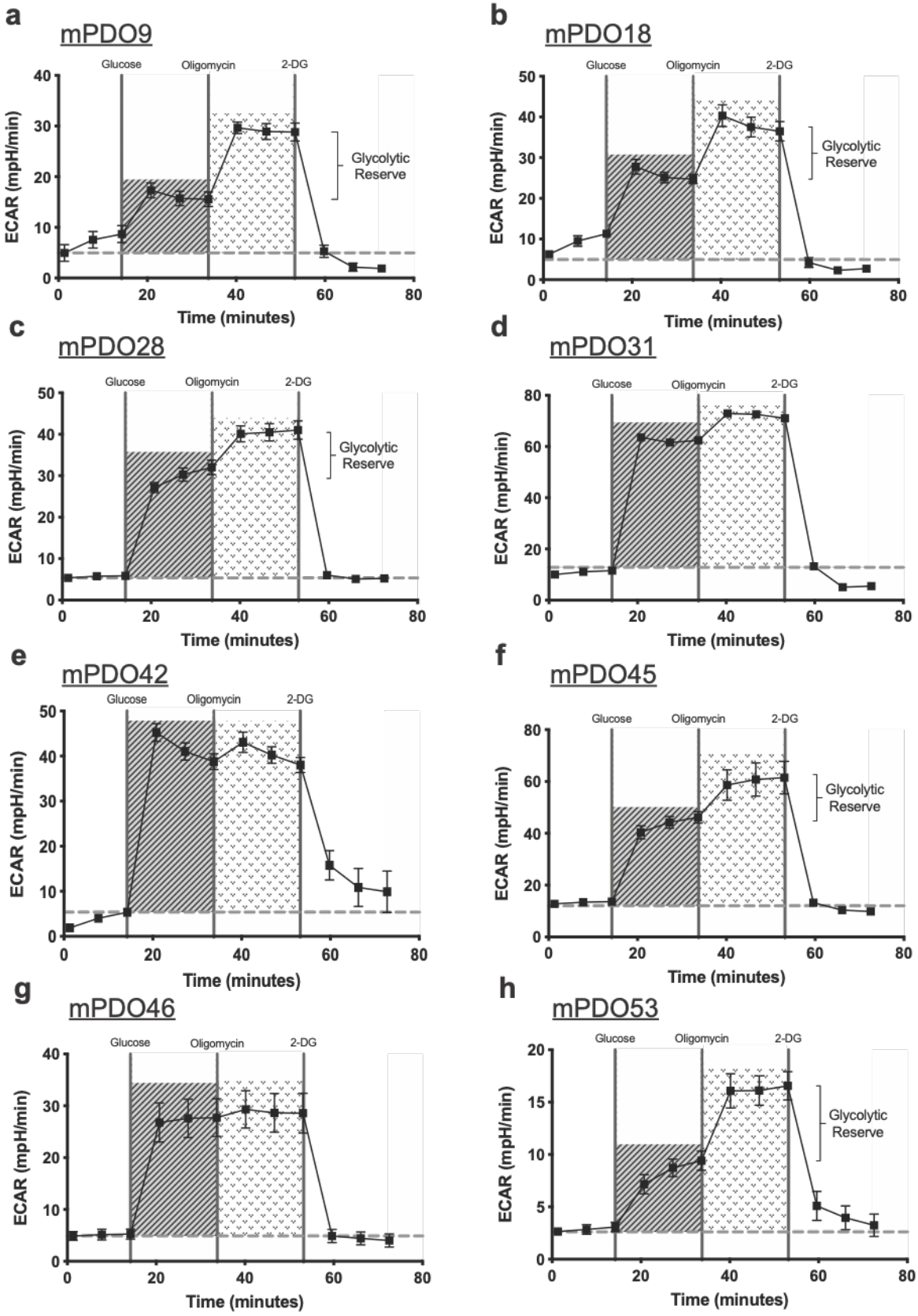
a
mPDO9
Glucose
Oligomycin
2-DG
Glycolytic Reserve
ECAR (mpH/min)
Time (minutes)
b
mPDO18
c
mPDO28
d
mPDO31
e
mPDO42
f
mPDO45
g
mPDO46
h
mPDO53

Figure 3.6: Baseline glycolysis measures in PDOs. (a-h) Measurement of extracellular acidification rate (ECAR) (mean ± SEM) in PDOs after injections of glucose, oligomycin and 2-DG during a glycolysis stress test. Glycolysis measurements show high variability in glycolytic reserves.

Table 3.1: Normalized glycolysis rates in untreated PDOs. Mean ECAR (mpH/min) values of basal glycolysis were subtracted from glycolytic capacity (GC), which is the maximum rate of glycolysis a PDO can achieve, to obtain glycolytic reserves (GR). Glycolytic reserves as proportions of glycolytic capacities are shown as GR/GC ratios.

PDO	Glycolysis (mpH/min)	Glycolytic Capacity (mpH/min)	Glycolytic Reserve (mpH/min)	GR/GC
mPDO9	8.62	21.11	12.49	0.59
mPDO18	15.25	27.16	11.91	0.44
mPDO28	26.17	35.23	9.06	0.26
mPDO31	36.48	36.65	0.17	0.00
mPDO42	38.97	36.2	0	0.00
mPDO45	32.48	47.84	15.36	0.32
mPDO46	22.71	24.34	1.63	0.07
mPDO53	10.66	18.48	7.82	0.42

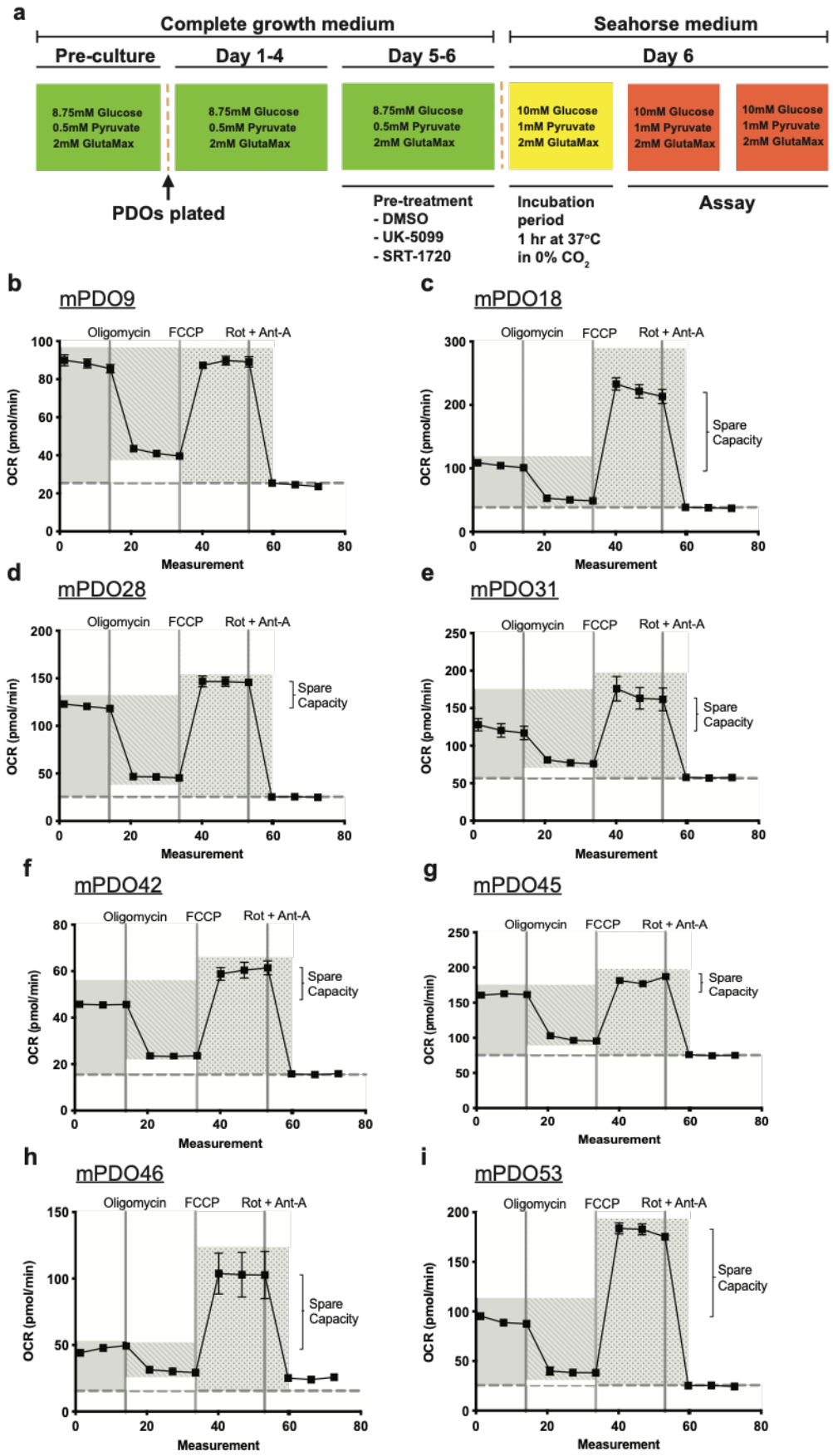
a
Complete growth medium
Seahorse medium
Pre-culture
Day 1-4
Day 5-6
Day 6
8.75mM Glucose
0.5mM Pyruvate
2mM GlutaMax
8.75mM Glucose
0.5mM Pyruvate
2mM GlutaMax
8.75mM Glucose
0.5mM Pyruvate
2mM GlutaMax
10mM Glucose
1mM Pyruvate
2mM GlutaMax
10mM Glucose
1mM Pyruvate
2mM GlutaMax
10mM Glucose
1mM Pyruvate
2mM GlutaMax
PDOs plated
Pre-treatment
- DMSO
- UK-5099
- SRT-1720
Incubation
period
1 hr at 37°C
in 0% CO2
Assay
b
mPDO9
c
mPDO18
d
mPDO28
e
mPDO31
f
mPDO42
g
mPDO45
h
mPDO46
i
mPDO53
Oligomycin
FCCP
Rot + Ant-A
OCR (pmol/min)
Measurement
Spare
Capacity

Figure 3.7: Baseline respiratory measures in PDOs. (a) Timeline of mito stress assay and changes in composition of media (b-i) Measurement of OCR (mean ± SEM) in PDOs after subsequent injections of oligomycin, FCCP and rotenone + antimycin-A during a mito stress test.

Table 3.2: Normalized respiration rates in untreated PDOs.

PDO	Basal (pmol/min)	Maximal (pmol/min)	ATP (pmol/min)	Spare Capacity (pmol/min)	SC/M
mPDO9	61.9	66.2	41.9	4.3	0.06
mPDO18	97.4	317.4	71.74	220	0.69
mPDO28	93.6	123.3	71.39	29.7	0.24
mPDO31	60.9	119.8	35.86	58.9	0.49
mPDO42	30.3	46.2	21.81	15.9	0.34
mPDO45	87.2	112.85	58.6	25.65	0.23
mPDO46	25.5	80.3	18.11	54.8	0.68
mPDO53	59.3	132.23	42.4	72.93	0.55

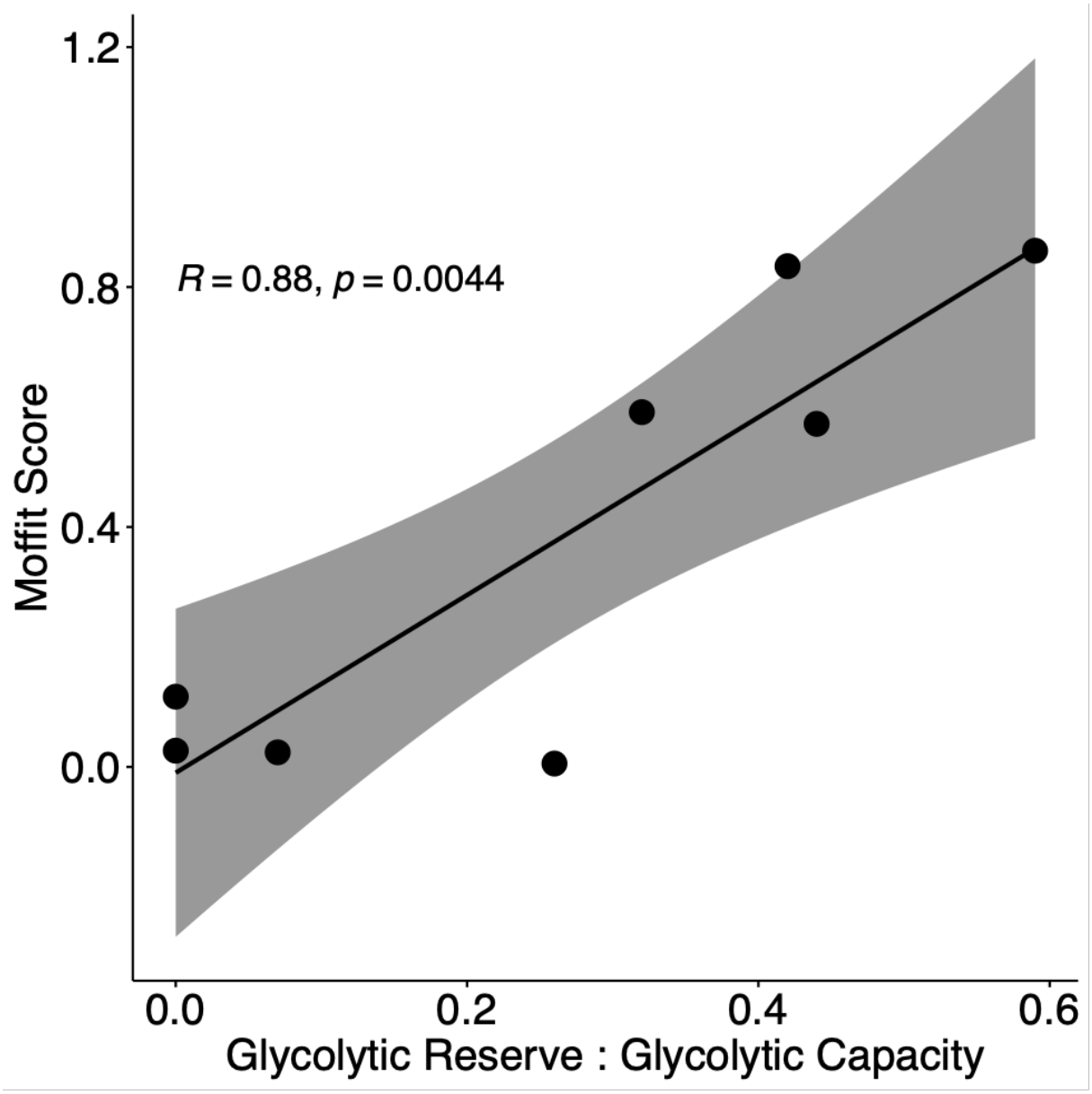

Figure 3.8: The ratio of glycolytic reserve to glycolytic capacity is positively correlated with Moffitt score. The Moffitt score is obtained from the weighted expression of 25 subtype signature genes per subtype (basal-like and classical). Scores over 0.88 are considered basal-like [29]. It increases with the proportion of glycolytic reserve to glycolytic capacity taken during baseline measurements. All ratio values are means of triplicates.

3.4 Induction and Quantification of Metabolic Flux by Targeting MPC1

Recently, Karasinska et al. [64] described four novel metabolic subtypes of PDAC. The glycolytic subtype was classified as having high expression of glycolytic and low expression of cholesterogenic genes. Glycolytic tumours associated with poor prognosis and the had lowest median overall survival. Further analysis showed that glycolytic tumours had the lowest expression of MPC1. A reduction in MPC1 expression and therefore MPC activity decreases influx of pyruvate into the mitochondria shifting tumour metabolism towards increased glycolysis and lowered OXPHOS. To better understand the role of MPC1 in metabolic reprogramming, we explored the effects of targeting MPC1 on tumour metabolism.

3.4.1 *Inhibition of MPC1 by UK-5099 Induces Glycolytic Hyperactivity in PDOs*

To investigate the phenotypic effect of inhibiting MPC1, PDOs were treated with UK-5099. UK-5099 is a potent inhibitor of MPC which inhibits the flow of pyruvate into the mitochondria (Figure 3.9a). This decrease in pyruvate flow consequently reduces any coupled OXPHOS activity [90, 91]. It was determined that 5 μM UK-5099 would be an optimal treatment dose, based on literature [92]. Glycolysis stress tests were performed on pretreated PDOs. UK-5099 raised basal glycolysis levels in 3/8 PDOs (Figure 3.10b, d and l) and glycolytic capacity in 4/8 PDOs (Figure 3.10b, d, j and n). Amongst PDOs that responded to treatment, the extent of increased glycolytic activity was variable with basal glycolytic increases up to ~100% and glycolytic capacity increases also up to ~100%. Comparing OCR:ECAR ratios shows no change during basal glycolysis for all but one PDO, mPDO53 where the ratio decreased post treatment (P= 0.036); and no change in glycolytic capacity in all but mPDO53 again, where the ratio decreased post

treatment as well (P=0.048) although the difference in mPO46 approached significance (P=0.057) (Figure 3.11a). Interestingly, we found 2/3 PDOs without a response had the lowest expression of Karasinska et al's glycolytic gene set and 2/2 of the most responsive PDOs, with increased glycolysis and glycolytic capacity, had the highest expression of glycolytic genes.

a

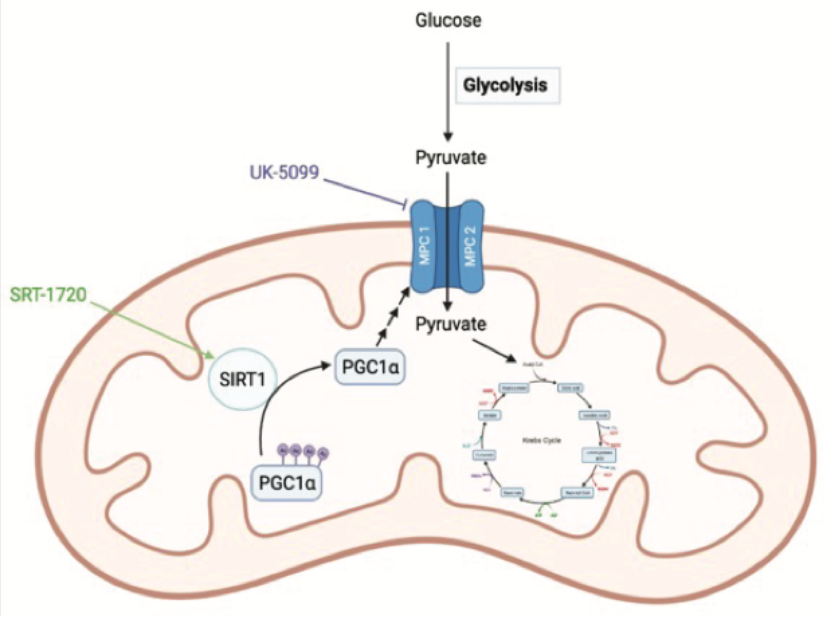
Glucose
Glycolysis
Pyruvate
UK-5099
MPC 1
MPC 2
SRT-1720
Pyruvate
SIRT1
PGC1α
PGC1α
Krebs Cycle

b

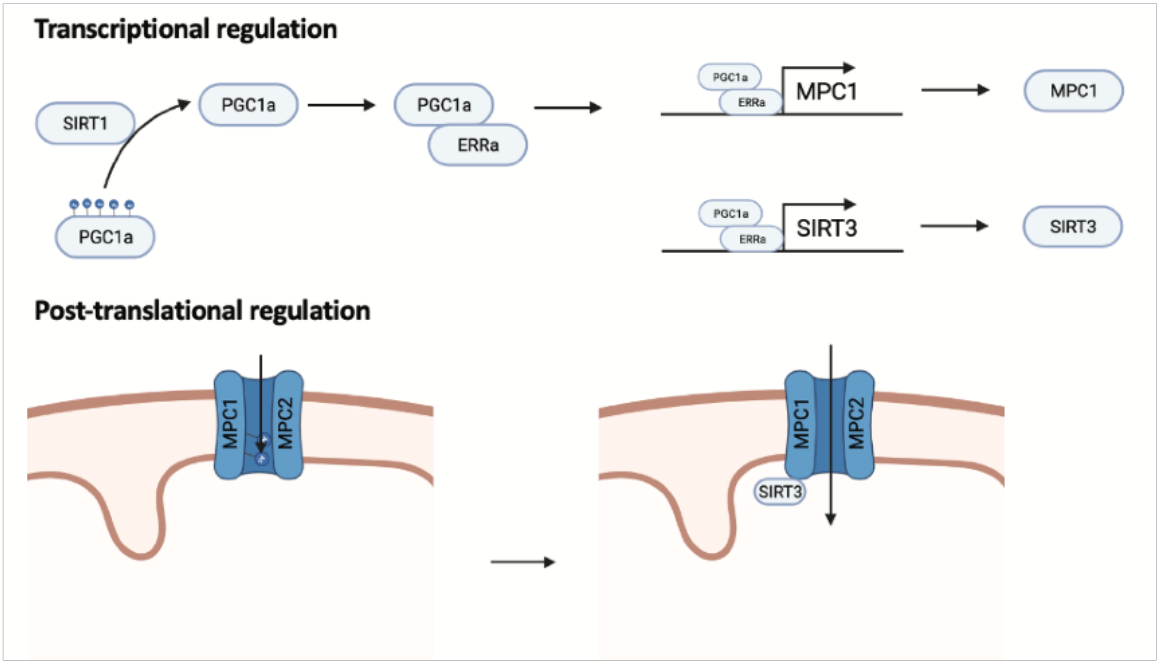
Transcriptional regulation
SIRT1
PGC1a
PGC1a
ERRa
PGC1a
PGC1a
ERRa
MPC1
MPC1
PGC1a
ERRa
SIRT3
SIRT3
Post-translational regulation
MPC1
MPC2
MPC1
MPC2
SIRT3

Figure 3.9: Targets and mechanisms of metabolic targeting compounds. (a) Direct targets of UK-5099 and SRT-1720 (b) Illustration of mechanisms by which SRT-1720 increases MPC1 activity.

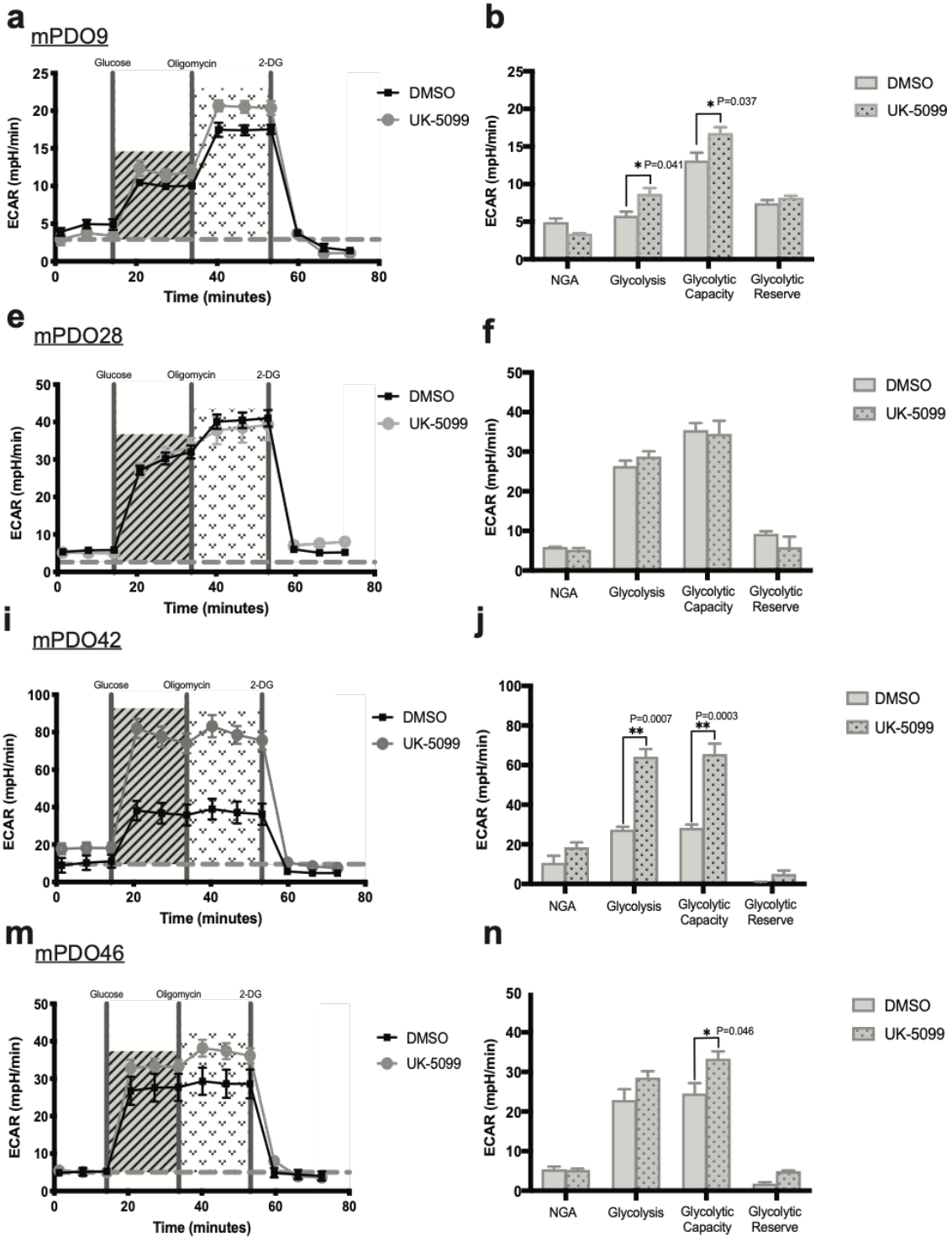
a
mPDO9
Glucose
Oligomycin
2-DG
ECAR (mpH/min)
Time (minutes)
DMSO
UK-5099
b
P=0.041
P=0.037
NGA
Glycolysis
Glycolytic Capacity
Glycolytic Reserve
e
mPDO28
f
i
mPDO42
P=0.0007
P=0.0003
j
m
mPDO46
P=0.046
n

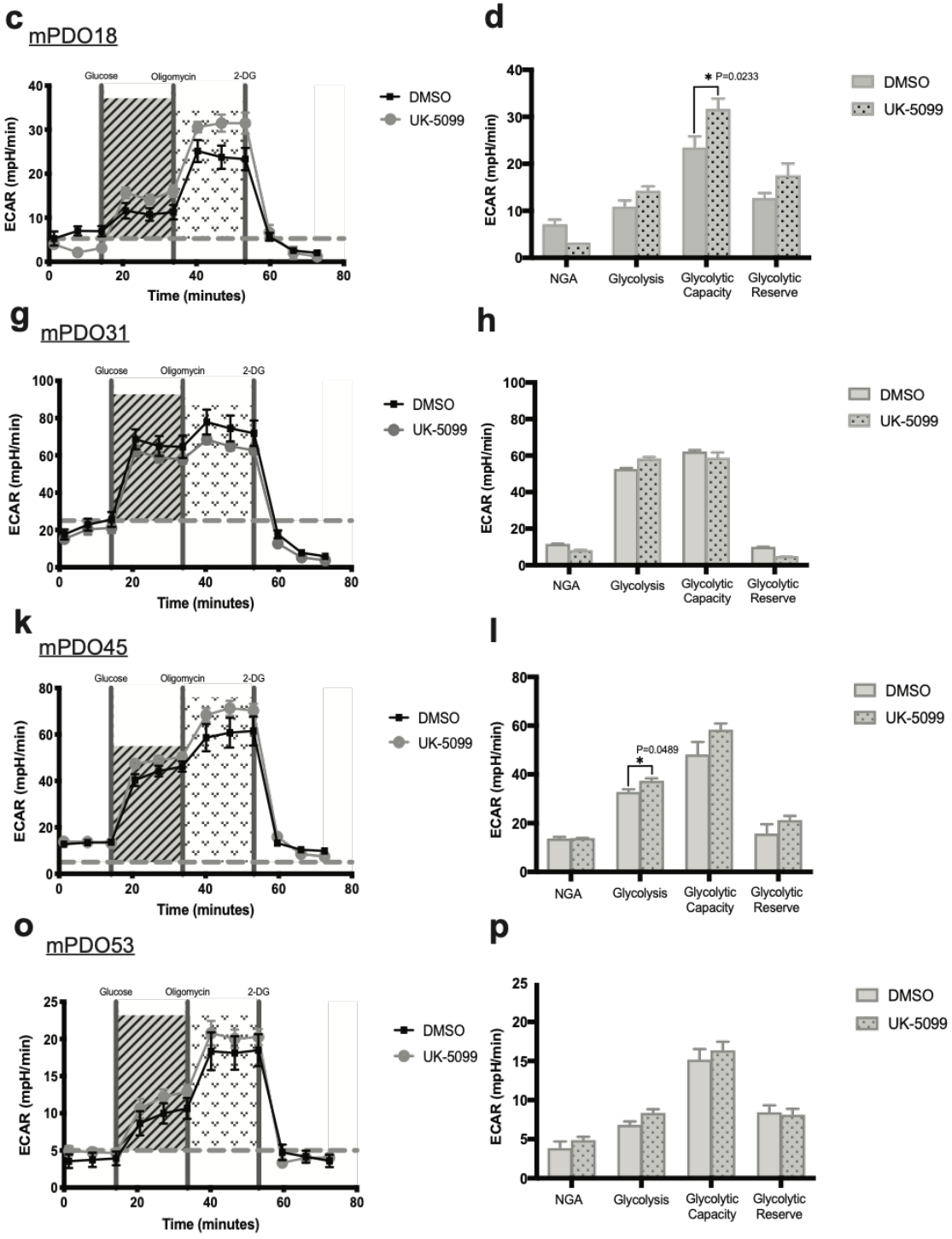
c
mPDO18
Glucose
Oligomycin
2-DG
ECAR (mpH/min)
Time (minutes)
DMSO
UK-5099
d
* P=0.0233
NGA
Glycolysis
Glycolytic Capacity
Glycolytic Reserve
g
mPDO31
h
k
mPDO45
P=0.0489
l
o
mPDO53
p

Figure 3.10: Quantification of glycolytic flux after treatment with UK-5099. (a-p) ECAR (mean ± SEM) obtained from glycolysis stress tests of PDOs treated with UK-5099 (5 μM) for 48 hours prior to assay. Differences in glycolysis were compared to dimethyl sulfoxide (DMSO) controls. (Student's t-test , *P<0.05, **P<0.001)

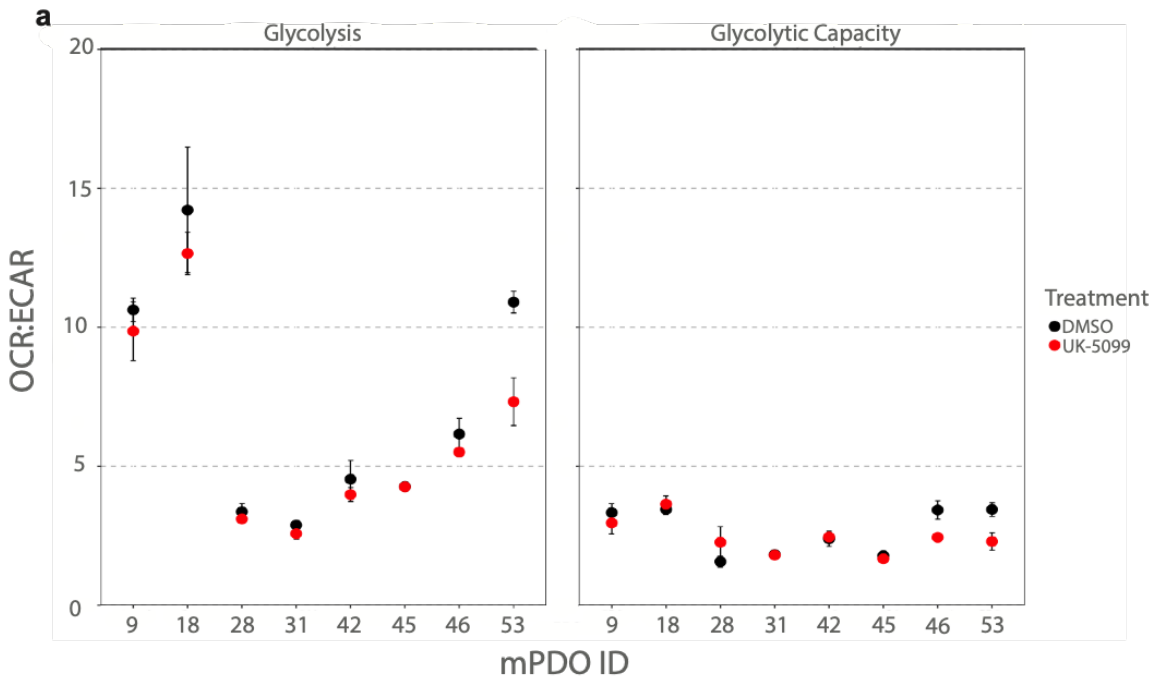
a
Glycolysis
Glycolytic Capacity
OCR:ECAR
20
15
10
5
0
9
18
28
31
42
45
46
53
mPDO ID
Treatment
DMSO
UK-5099

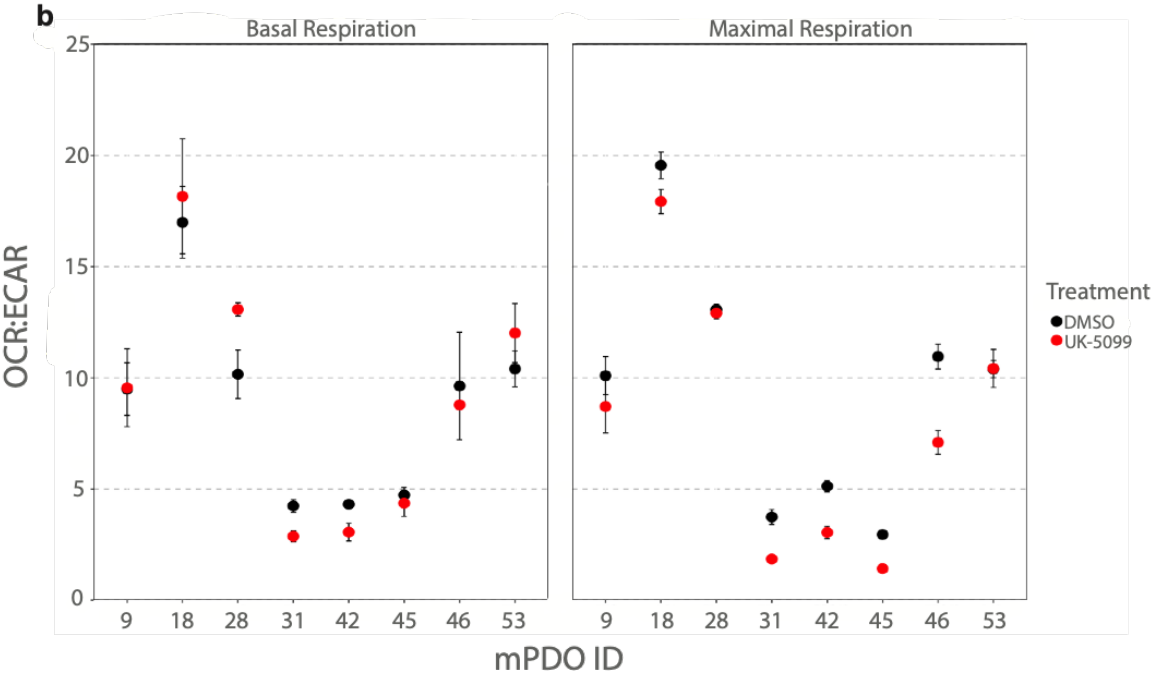
b
Basal Respiration
Maximal Respiration
OCR:ECAR
25
20
15
10
5
0
9
18
28
31
42
45
46
53
mPDO ID
Treatment
DMSO
UK-5099

Figure 3.11: Comparison of OCR:ECAR ratios in PDOs treated with UK-5099. (a) Shifts in OCR:ECAR (mean ± SEM) occurring during baseline glycolysis and at glycolytic capacity (b) Shifts in OCR:ECAR occurring during baseline respiration and at maximal respiration.

3.4.2 *Inhibition of MPC1 by UK-5099 Reduces Respiratory Capacity in PDOs*

We next sought to capture the effect of inhibiting MPC1 on OXPHOS activity. Given that inhibiting MPC1 would block pyruvate influx to the mitochondria, we hypothesized a net reduction in respiratory measurements. Mito stress tests were performed on PDOs treated with 5 μM UK-5099. Treatment decreased basal OXPHOS rates in 5/8 PDOs (Figure 3.12b, f, j, g and k) and more strikingly, decreased maximal respiration rates in 7/8 PDOs (Figure 3.12b, f, j, d, h, l and p). Amongst PDOs basal respiration reductions ranged from 18-32% and maximal respiration was reduced by ~50% on average. Comparing OCR:ECAR ratios there was no change for basal respiration in all but one PDO, mPDO31 which had a reduced ratio (P=0.0147); maximal respiration were increasingly reduced with reduction in mPDO31 (P=0.0075), mPDO42 (P=0.0053), mPDO45 (P=6.845x10^{-5}) and mPDO46 (P=0.038) (Figure 3.11b).

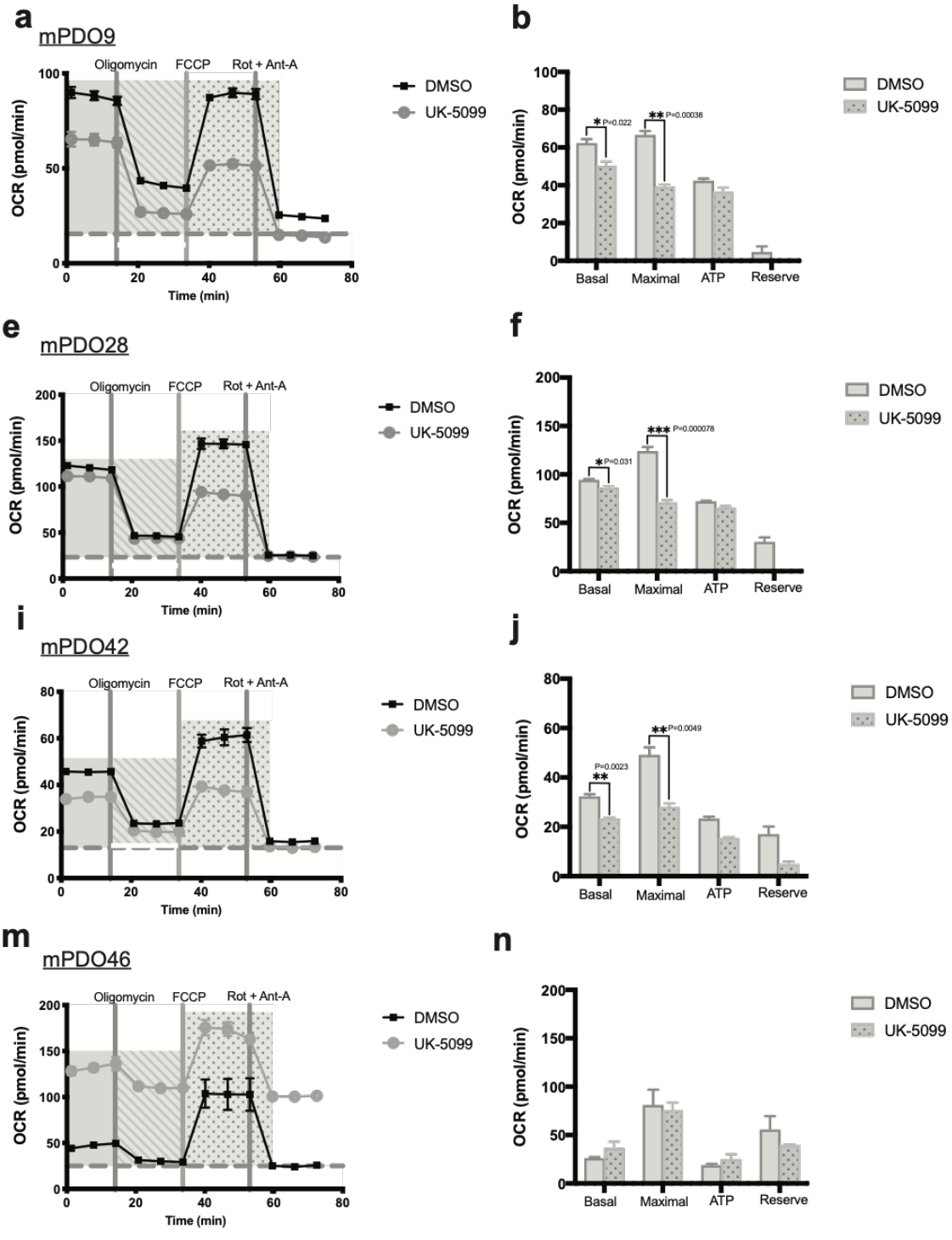
a
mPDO9
Oligomycin
FCCP
Rot + Ant-A
OCR (pmol/min)
Time (min)
DMSO
UK-5099
b
OCR (pmol/min)
*P=0.022
**P=0.00038
Basal
Maximal
ATP
Reserve
DMSO
UK-5099
e
mPDO28
Oligomycin
FCCP
Rot + Ant-A
OCR (pmol/min)
Time (min)
DMSO
UK-5099
f
OCR (pmol/min)
*P=0.031
***P=0.000078
Basal
Maximal
ATP
Reserve
DMSO
UK-5099
i
mPDO42
Oligomycin
FCCP
Rot + Ant-A
OCR (pmol/min)
Time (min)
DMSO
UK-5099
j
OCR (pmol/min)
**
P=0.0023
**P=0.0049
Basal
Maximal
ATP
Reserve
DMSO
UK-5099
m
mPDO46
Oligomycin
FCCP
Rot + Ant-A
OCR (pmol/min)
Time (min)
DMSO
UK-5099
n
OCR (pmol/min)
Basal
Maximal
ATP
Reserve
DMSO
UK-5099

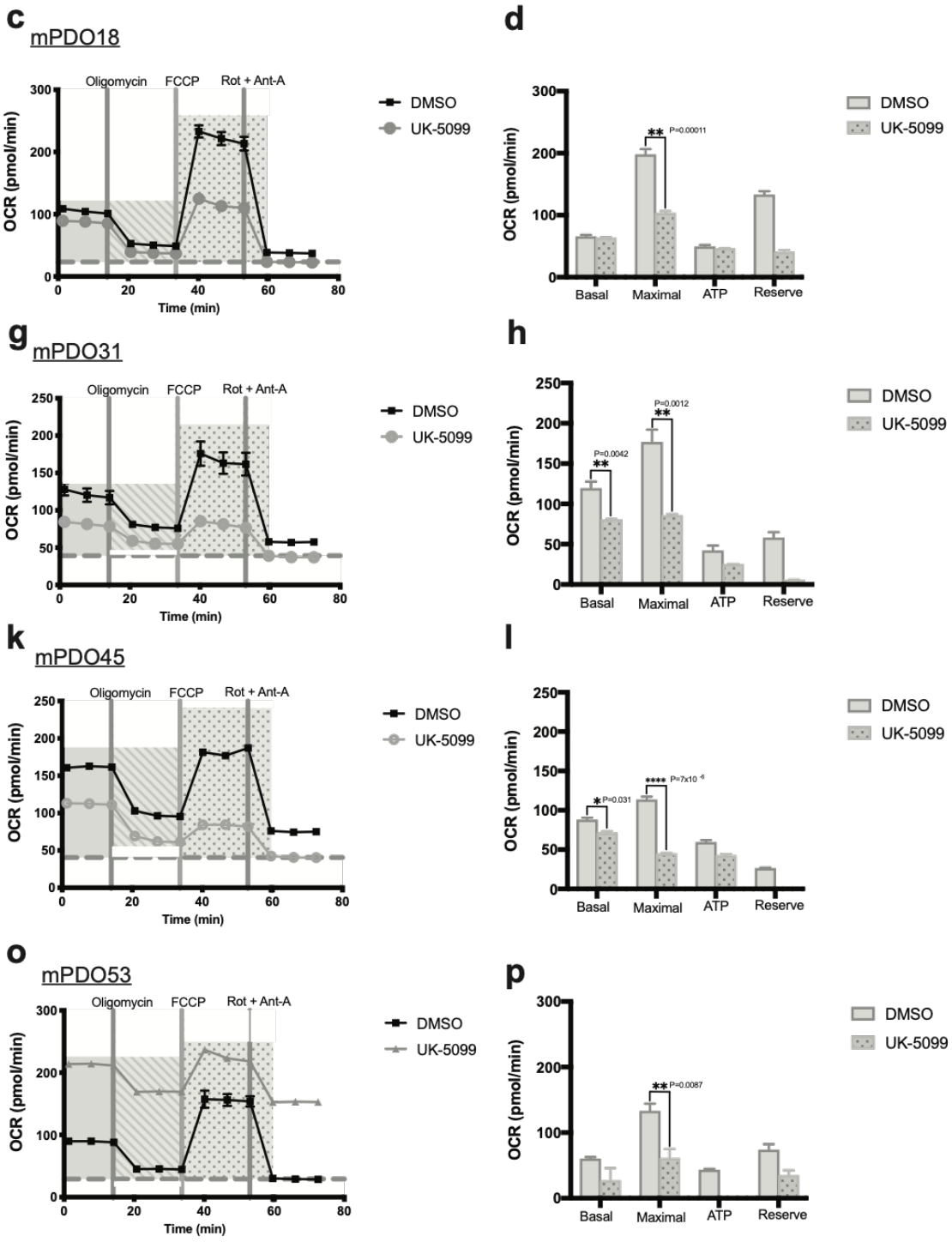
c
mPDO18
Oligomycin
FCCP
Rot + Ant-A
OCR (pmol/min)
Time (min)
DMSO
UK-5099
d
P=0.00011
Basal
Maximal
ATP
Reserve
g
mPDO31
P=0.0042
P=0.0012
h
k
mPDO45
l
P=0.031
P=7x10 -6
o
mPDO53
p
P=0.0087

Figure 3.12: Quantification of respiratory flux after treatment with UK-5099. (a-p) OCR (mean ± SEM) from mito stress tests of PDOs treated with UK-5099 (5 μM) for 48 hours prior to assay. Differences in oxygen consumption were compared to DMSO controls. (Student's t-test, *P<0.05, **P<0.005, ***P<0.0001, ****P<$0.1x10^{-5}$)

3.4.3 *Activation of PGC1α by SRT-1720 Reduces Peak Glycolysis in Some PDOs*

To further study the malleability of these metabolic processes, PDOs were treated with the compound SRT-1720. A compound that has been shown to decrease the ratio of anerobic to aerobic respiration [93]. SRT-1720 activates SIRT1 (Figure 3.9a), a NAD-dependent histone deacetylase. SIRT1 regulates glucose and lipid metabolism through its deacetylase activity for over two dozen substrates [94]; one of which is the PGC1α [95]. PGC1α is a transcriptional coactivator, upon deacetylation by SIRT1, forms a complex with ERRα. This complex has been shown to upregulate transcription of MPC1 in breast cancer [96] (Figure 3.9b). Furthermore, the PGC1α/ERRα complex also upregulates the transcription of SIRT3. SIRT3 has been reported to deacetylate and bind MPC1 thereby stabilizing it (Figure 3.9b) [97], and stimulate mitochondrial biogenesis [98]. To this end, we treated PDOs with 2.5-5 μM of SRT-1720 depending on their pre-determined tolerable doses. Glycolysis stress tests were then performed on this cohort. Glycolysis remained unchanged in all PDOs (Figure 3.13a-l) and glycolytic capacity was reduced in 2/6 PDOs (Figure 3.13f and l). Comparing OCR:ECAR ratios shows no significant differences in basal glycolysis. Although a difference in glycolytic capacities was observed for some, statistical significance was reached for mPDO53 which had a reduced ratio(P=0.00684). (Figure 3.14a). The findings in this experiment indicate that while SRT-1720 decreases the cytoplasmic pyruvate pool in some PDOs, we cannot determine if this reduction is due to increased mitochondrial influx.

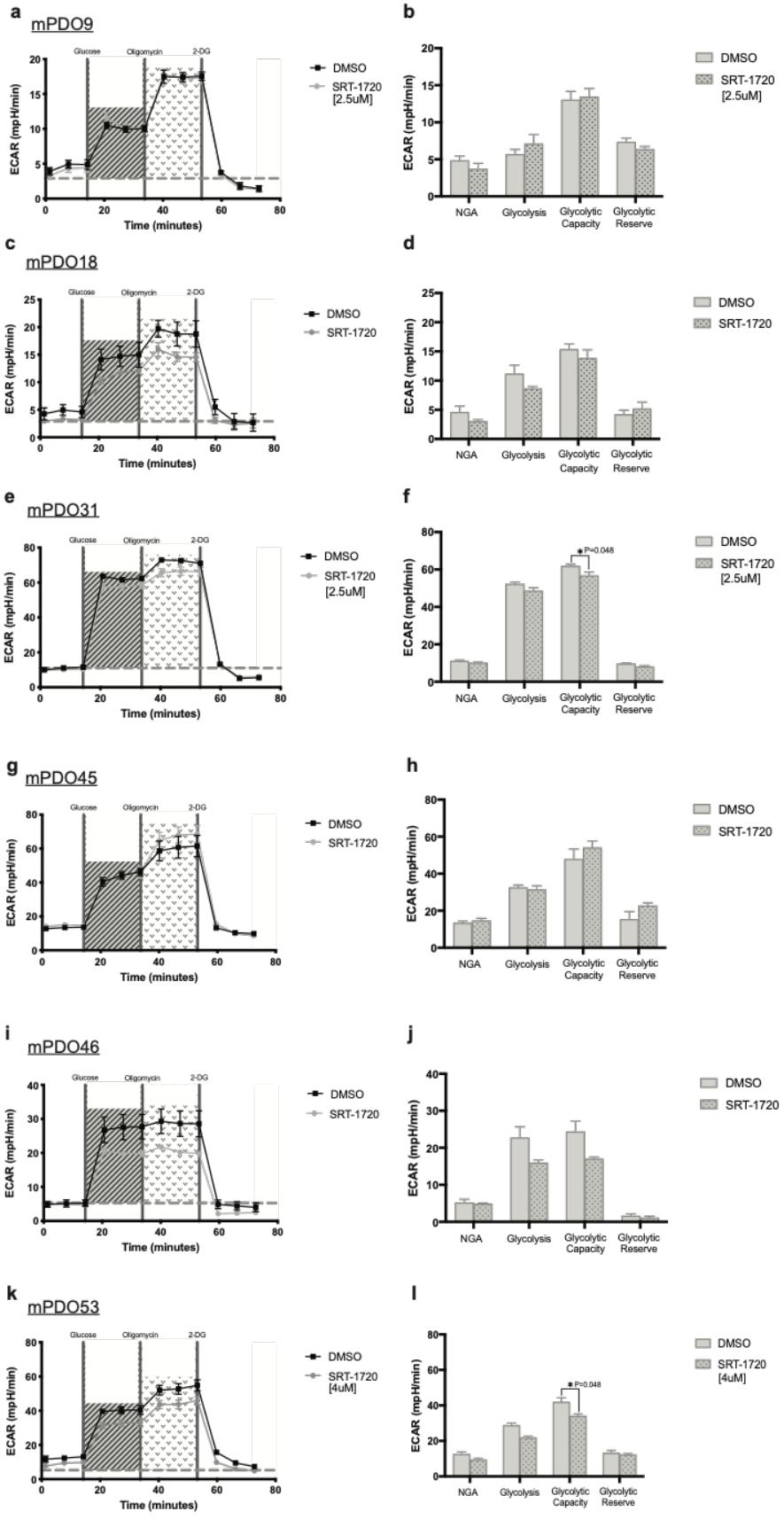
a
mPDO9
Glucose
Oligomycin
2-DG
ECAR (mpH/min)
Time (minutes)
DMSO
SRT-1720 [2.5uM]
b
NGA
Glycolysis
Glycolytic Capacity
Glycolytic Reserve
c
mPDO18
SRT-1720
d
e
mPDO31
f
*P=0.048
g
mPDO45
h
i
mPDO46
j
k
mPDO53
SRT-1720 [4uM]
l

Figure 3.13: Quantification of glycolytic flux after treatment with SRT-1720. (a-p) ECAR (mean ± SEM) values from glycolysis stress tests of PDOs treated with SRT-1720 (2.5-5 μM) for 48 hours prior to assay. Differences in glycolysis were compared to DMSO controls. 5 μM SRT-1720 used unless specified otherwise. (Student's t-test, *P<0.05)

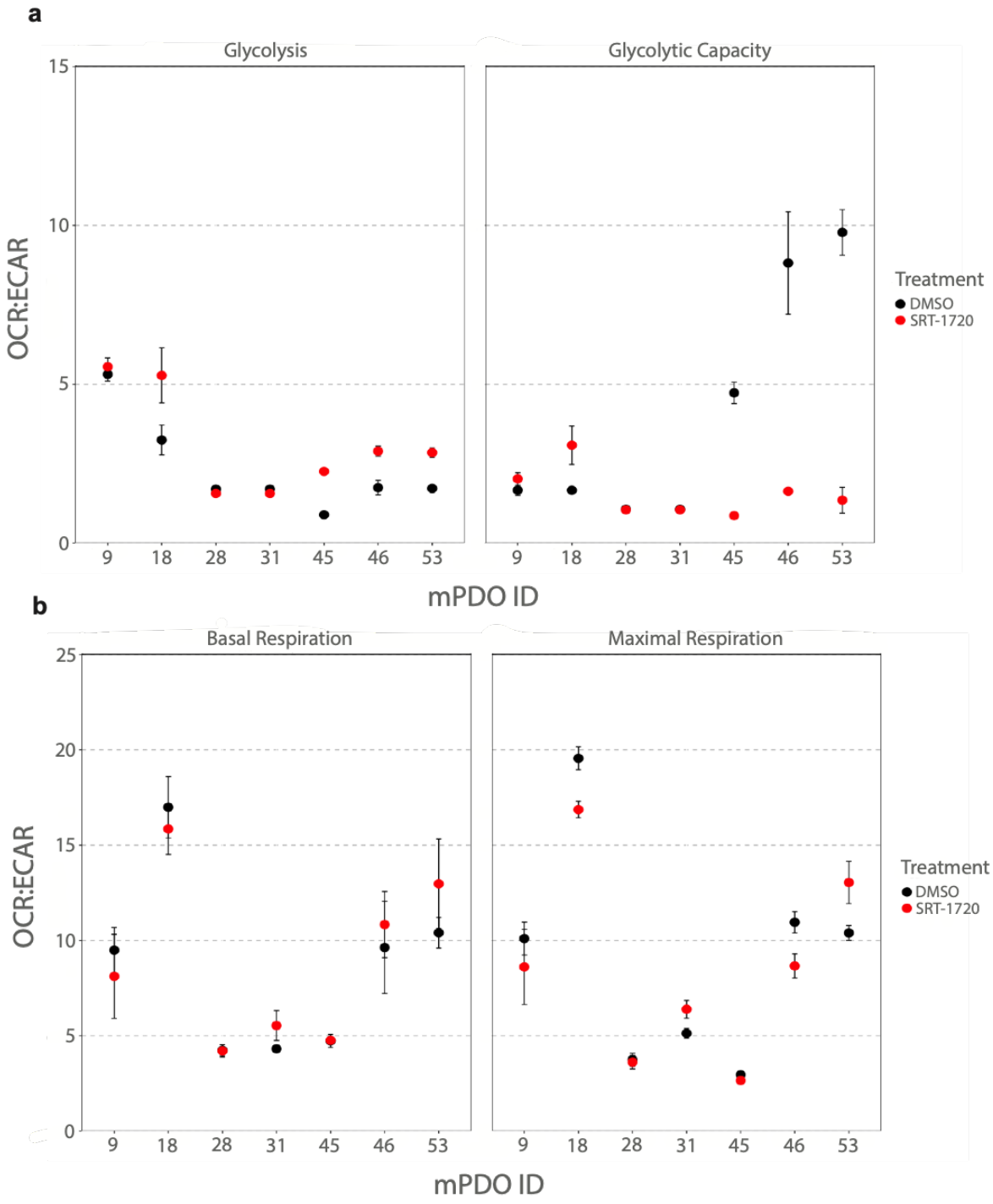
a
Glycolysis
Glycolytic Capacity
OCR:ECAR
15
10
5
0
9
18
28
31
45
46
53
mPDO ID
Treatment
DMSO
SRT-1720
b
Basal Respiration
Maximal Respiration
OCR:ECAR
25
20
15
10
5
0
9
18
28
31
45
46
53
mPDO ID
Treatment
DMSO
SRT-1720

Figure 3.14: Comparison of OCR:ECAR ratios in PDOs treated with SRT-1720. a) Shifts in OCR:ECAR (mean *pm* SEM) occurring during baseline glycolysis and at glycolytic capacity (b) Shifts in OCR:ECAR occurring during baseline respiration and at maximal respiration

3.4.4 *Effects of Activating PGC1α on OXPHOS in PDOs*

Given the reduction in glycolysis levels following PGC1α activation (Figure 3.9b), we next sought to determine the effect on OXPHOS rates. PDOs were treated with 2.5-5 μM of SRT-1720 and mito stress tests were performed (Figure 3.15a-n). There was no change in basal respiration and maximal respiration in all but one PDO, mPDO9 (Figure 3.15a) which had decreased basal (P=0.021) and maximal respiration (P=0.012) without any evidence of reduction occurring due to cell death. However, mPDO9 has shown to have increased sensitivity to SRT-1720, having a lower tolerable dose compared to the rest so it is possible that the PDOs are in a critical state preceding cell death. A comparison of OCR:ECAR ratios shows no shifts during basal respiration. Similarly, maximal respiration remained unchanged in all but mPDO18, where it decreased (P=0.013) (Figure 3.14b). While a reduction in glycolysis was observed in some PDOs, these data suggest that this change is not caused by an influx of pyruvate into the mitochondrion. Rather, the decrease in ECAR could be due to a damping effect on glycolysis by SRT-1720.

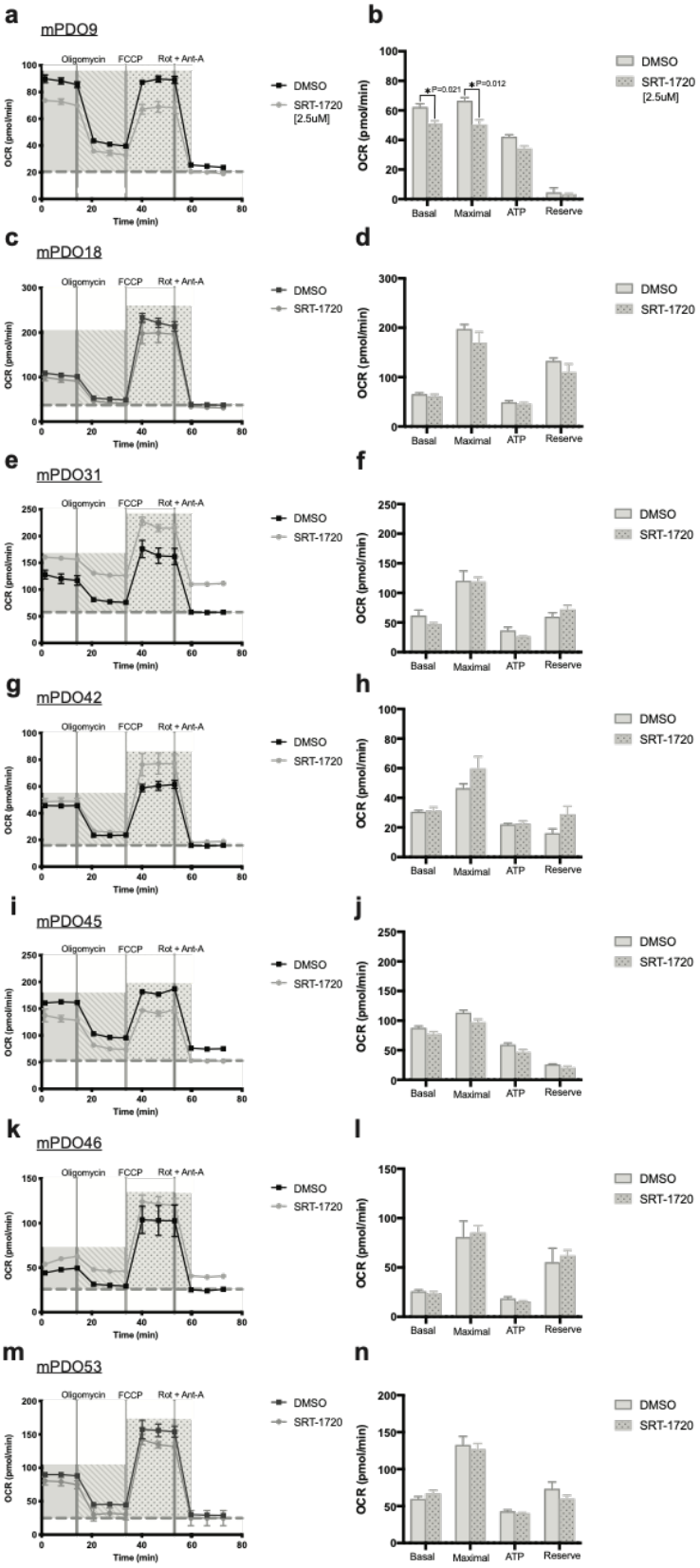
a
mPDO9
Oligomycin
FCCP
Rot + Ant-A
OCR (pmol/min)
Time (min)
DMSO
SRT-1720 [2.5uM]
b
*P=0.021
*P=0.012
Basal
Maximal
ATP
Reserve
c
mPDO18
d
e
mPDO31
f
g
mPDO42
h
i
mPDO45
j
k
mPDO46
l
m
mPDO53
n

Figure 3.15: Quantification of respiratory flux after treatment with SRT-1720. (a-p) OCR (mean ± SEM) from mito stress tests of PDOs treated with SRT-17200 (2.5-5 ±M) for 48 hours prior to assay. Differences in glycolysis were compared to DMSO controls. 5 μM SRT-1720 used unless specified otherwise. (Student's t-test, *P<0.05)

Chapter 4: Discussion

PDAC tumours exhibit a high degree of intertumoral heterogeneity. Classifications of PDAC into multiple transcriptomic molecular and metabolic subtypes highlight the presence of different tumoral subpopulations and suggests that their metabolism is deferentially modified [64]. Here, we quantified the metabolic phenotypes of PDOs and sought to shift their metabolism to an alternative state by targeting MPC1. MPC1 is one of two protomers of MPC for which over 60% of PDAC experience a heterozygous loss. Leveraging the Seahorse XFe96 analyzer, we captured metabolic snapshots of a cohort of eight PDOs representing a diverse range of molecular and metabolic subtypes. To be able to measure metabolic flux in PDOs, we adapted the seahorse platform for maximum compatibility with PDOs. Together, my results provide a novel phenotypic insight of inter-mPDO variance during glycolysis and OXPHOS and how targeting MPC1 can induce metabolic flux. PDOs chosen for this represented a full array of molecular and metabolic subtypes.

Cellular metabolism is a dynamic process constantly adjusting for stresses caused by nutrient depletion and anabolic demands [99]. Growth constraints by the pancreatic tumour microenvironment cause the cell to undergo metabolic rewiring, considered a hallmark of oncogenesis [100], to enable rapid proliferation and growth. Several groups have stratified PDAC based on the expression of metabolic genes into metabolic subtypes [49, 64]. Here, we translate these findings by profiling basal levels of glycolysis and OXPHOS using PDOs. The seahorse glycolysis and mito stress test assays were used to obtain these measurements. The seahorse assays and microplate were developed for 2D cells and required adaptation for use with PDOs.

My approach to this was based on the consideration of: (i) ensuring the Matrigel layer was sufficient to allow PDO formation (ii) the Matrigel layer did not interfere with device sensors (iii) PDOs required higher compound concentrations than 2D cultured cells (iv) minimizing the effect of ECM decreased compound diffusion coefficients [101] on PDOs (v) the need for pre-assay PDO quantification for post-hoc analysis.

We performed baseline metabolic measurements on treatment naive PDOs. Glycolytic measurements showed the extent of the Warburg effect; there was a large variance in glycolytic reserves amongst PDOs highlighting the extent of differential metabolic reprogramming. We observed that 3/8 PDOs had low and 5/8 PDOs had moderate to high glycolytic reserves present. Furthermore, three PDOs with highest reserves classified as basal-like and five with moderate to low reserves classified as classical; these latter PDOs appear to reach and function near maximum glycolytic capacity indicating high demand for pyruvate and/or NADH. A comparison of ECAR values between PDOs could be confounded by batch effects. To reliably compare PDOs, we used glycolytic reserve to glycolytic capacity ratios which showed a strong positive correlation with Moffitt subtype scores (R=0.86, P=0.0067). These data suggest the notion that the ability to upregulate glycolysis is increased in PDOs with basal-like gene expression patterns. This increased glycolysis buffer may allow these tumours to better adapt to reduced nutritional availability. Respiratory measurements showed the extent of variability in both baseline and maximal respiration rates. Although there were no correlates to subtypes, we observed that the PDO (mPDO9) with the highest baseline respiratory rate was also the highest expressor of cholesterogenic and glycolytic gene sets; also indicating high dependence on pyruvate for lipid biosynthesis. This PDO had virtually no spare respiratory capacity and further analysis showed this to be the only one to have a PDK1 copy number gain. Increased

PDK would reduce pyruvate conversion into Acetyl-CoA creating a bottleneck effect decreasing the ability to regulate OXPHOS rates when needed [102]. Loss of TP53 is known to inhibit OXPHOS and concurrently stimulate glycolysis [103], KRAS mutations have been shown to have similar effects [104]; a comparison of two PDOs (mPDOs 42 and 46) from our cohort with both having wild type TP53 but only one of them with wildtype KRAS (mPDO42) shows decreased dependence on OXPHOS in the KRAS mutant PDO (Figure 3.7). Biopsies from which PDOs with high glycolytic reserves were shown to have high expression of main glycolysis pathway genes such as GAPDH and TPI. GAPDH is a rate limiting enzyme in aerobic glycolysis [105], high expression of which associates with increased metastatic and a more aggressive phenotype [106]. Inactivating TPI during oxidative stress is crucial in mediating a protective metabolic configuration [107]. High TPI expression is associated with high proliferation and metastasis rates [108]. As such, future studies may seek to explore trends in respiratory rates and gene expression patterns to better understand the functional relevance of deferentially expressed genes and to explore genomic mechanisms by which these metabolic processes are regulated. Taken together, these results suggest that PDOs have distinct metabolic profiles whereby some PDOs are able to increase both glycolysis and OXPHOS; and others only one.

Successful metabolic measurements necessitate a few technical trade-offs. For instance, the PDOs I used, although being able to capture host tumour histopathological and genomic features, are devoid of tumour stroma potentially reversing or causing additional metabolic rewiring based on artificial growth conditions. These PDOs were grown atop an ECM layer which, although porous, reduces diffusion rates potentially delaying the effects of assay compounds and having a variable effect based on PDO exposure potentially altering metabolic readouts; compounds were used at

saturating concentrations discordant from in vivo conditions; and the imaging-based cell quantification approach was limited to a single z-plane for a three-dimensional model, combined with variable drug effect based on exposure of PDOs could result in inaccurate normalization of readouts. It is technically challenging to determine accurate and true ECAR and OCR rates, the seahorse analyzer measures ECAR based on lactate-coupled proton extrusion without considering the buffering capacity of media, mitochondrial CO_2 proton release and the pentose phosphate pathway. Measured OCR rates aren't inclusive of substrate level phosphorylation driven by glutamine [109, 110].

Having successfully generated a mini atlas of metabolic measurements in PDOs provided an opportune moment to exploit key targets and alter levels of metabolic reprogramming. Loss of MPC1, one of two protomers forming the functional MPC, contributes to tumour progression. A growing body of evidence suggests MPC1 is downregulated in multiple cancer types such as colorectal, gastric, liver and lung [111] and over 60% of metastatic PDAC patients experience a copy loss [64]. This suppression of MPC1 reenforces the Warburg phenotype [112]. While the effect of inhibiting MPC1 has been studied before in other cancer types [112, 113], we were able to extend these to PDAC focusing on both glycolysis and OXPHOS. Changes in glycolysis and OXPHOS were determined in response to the MPC1 inhibitor UK-5099. UK-5099 was able to upregulate glycolysis and/or glycolytic capacity in select PDOs (Figure 3.10) irrespective of their metabolic or molecular subtype. These changes were recorded after the compound was removed 1.5-2 hours prior to the assay indicating that metabolic reprogramming had indeed been altered. It is possible that other PDOs responded to UK-5099 as well but underwent a reversal upon removal. Next, we assessed the effects of UK-5099 on OXPHOS rates and showed reduced maximal

respiration rates in 7/8 PDOs. Although the primary route for mitochondrial pyruvate entry is the MPC1/MPC2 heterodimer, MPC2 has been shown to form functional homodimers [114]. These results indicate that MPC2 homodimers are not able to sufficiently handle increased pyruvate traffic. A possible reason for the lack of response by mPDO53 could be that it is the highest expresser of MPC1L, a less common paralog of MPC1, amongst the cohort. MPC1L has been shown to form functional heterodimers with MPC2 and although these too are inhibited by UK-5099 under saturating conditions [109], the relative extent of inhibition by the dose of UK-5099 given remains unclear. Additionally, pyruvate can bypass MPC by getting converted to alanine which then enters the mitochondria via alanine aminotransferase [115] and is converted back to pyruvate [116].

Through inhibition of MPC1, we were able to validate that the modified seahorse assay was sensitive enough to detect metabolic changes. In a study of tissue microarray data from resected PDAC patients, reduced MPC1 protein levels associated with reduced survival [113]. Re-expression of MPC1 has also been shown to lower glycolysis [108]. Hence, we sought to pharmacologically increase OXPHOS levels using SRT-1720, which has been shown to increase MPC1 expression [66]. SRT-1720 is an activator of SIRT1 [117], activated SIRT1 then goes onto deacetylate PGC1α [65, 93, 118] which forms a complex with ERRα in the proximal MPC1 promoter resulting in increased MPC1 expression [66]. We show that SRT-1720 decreased the glycolytic capacity of 2/6 PDOs and this reduction approached significance in a third one. Next, we were curious if SRT-1720 treatment would raise OXPHOS rates. However, OXPHOS rates remained unaltered with the exception of one PDO, which strangely had decreased OXPHOS levels. These data generate questions that will benefit from future research, such as how MPC1 levels are affected by activating PGC1α in PDOs and which subcellular

compartment is pyruvate relocated to, if not the mitochondria.

Chapter 5: Conclusion

5.1 Summary and Significance of Findings

PDAC has been stratified into multiple genomic and transcriptomic subtypes. These classifications are based on the weighted differential expression of genes amongst patient tumours, which are used to assign signatures scores [51, 54, 64]. These molecular and metabolic subtypes provide insights into pathway modifications that aid in tumour progression. One such pathway is glycolysis, which is increased in PDAC tumours, known as the Warburg effect [58]. Our group previously showed that in metastatic PDAC MPC1 is deleted in over 60% of tumours and that the glycolytic subtype has the lowest expression of MPC1 [64]. Here we sought to reduce tumour aggressiveness by targeting MPC1. This thesis had three major objectives. First, to establish an assay to measure baseline tumour metabolism and metabolic flux in PDOs. Second, investigate baseline levels of glycolysis and OXPHOS in PDOs. Last, investigate the effect of targeting MPC1 and tumour metabolism in PDOs. To assess tumour metabolism, we utilized PDOs as our model system. PDOs are able to recapitulate donor tumour histopathological and genomic features and thus enable assessment of tumour metabolism. A novel aspect of this work was our ability to precisely measure PDAC PDO metabolism. We adapted the Seahorse XFe96 analyzer for use with PDOs and measured metabolism with low inter-experimental and inter-replicate variance. We characterized basal metabolism in a cohort of eight PDOs. Glycolytic measurements showed high variation in glycolytic reserves. However, PDOs with high reserves did not necessarily have high basal glycolysis rates indicating that certain tumours reprogrammed their metabolism to have a higher bandwidth for glycolysis and that

this glycolytic program could be required for the tumour to survive and propagate in the host. We were able to associate metabolic gene expression with underlying in vitro metabolism, further improving our understanding of the functional role differential gene expression play in tumour metabolism and the relevance of PDAC subtypes. When glycolytic reserves as proportions of glycolytic capacities were compared to Moffitt signature scores, a significantly positive correlation was observed. These findings indicate that PDOs with higher reserves also had higher Moffitt scores, indicating a tendency to have a basal-like tumour subtype. Biopsies from which these high reserve tumours were derived had high expression of glycolysis pathway genes associated with aggressive disease. Next, we showed the plasticity in metabolic reprogramming by targeting MPC1. Inhibition of MPC1 resulted in a near unanimous (7/8) decrease of OXPHOS while increasing peak glycolysis in 4/8 PDOs . These findings suggest that in PDOs with low basal glycolysis, reducing ATP production via MPC1 inhibition creates a surge in demand to which cells respond by rewiring metabolism to increase glycolytic capacity. Furthermore, PDOs were treated with SRT-1720, an activator of SIRT1 which through PGC1α has been shown to increase MPC1 transcription [66]. SRT-1720 treatment did not increase OXPHOS in any PDO although glycolytic capacity was decreased in 2/6 PDOs. These results suggest that SRT-1720 does reduce the pyruvate pool in some PDOs but that is not due to flow of pyruvate into the mitochondria, thus challenging the notion of SRT1 mediated MPC1 increase. While the effects of pharmacologically increasing MPC1 activity in PDOs require further study, this thesis provides the groundwork to quantify the effects of metabolism targeting agents allowing for the development of novel metabolic therapies for PDAC.

5.2 Limitations

Although treatment with UK-5099 caused metabolic flux in some PDOs, a major limitation of these results is the removal of drug before the assay. In PDOs without a response to UK-5099, we were not able to definitively determine if lack of response was due to resistance to drug or inability to increase glycolysis. Similarly, due to the mixed response in PDOs treated with SRT-1720, we were not able to definitively determine if the lack of response was due to resistance or insufficient increase in MPC1 levels. Furthermore, due to the complete lack of response in respiratory measures, it is possible that SRT-1720 is not able to sufficiently raise MPC1 levels. Lastly, a major limitation of this study is that changes in MPC1 protein levels were not able to be adequately quantified in treated PDOs as the magnitude of change, if any, was likely below the threshold of detection of a western blot.

5.3 Future Directions

There remain opportunities to study the effect of targeting MPC1 on metabolism. Given that activating PGC1α causes a transcriptional increase in MPC1, PDOs could be treated with lower dose of SRT-1720 for a longer time period or perhaps even cultured in SRT-1720 for a limited time prior to measurements. Such a transcriptional increase in MPC1 could affect PDO growth rates which need to be quantified. Another priority is quantifying this change in MPC1 expression and the resultant protein product. Regarding reducing glycolysis, we observed a reduction in glycolytic capacity in two PDOs after SRT-1720 treatment, exploring the mechanistic cause of this change could elucidate vulnerabilities in resistance. Furthermore, a metabolite tracing study could be used to identify the compartments receiving extra pyruvate. PDOs with a high

glycolytic reserves and therefore high GAPDH could be targeted using vitamin C which has been shown to selectively kill KRAS mutant tumours by targeting GAPDH [119]. While this thesis was focused on targeting MPC1, additional agents to regulate metabolism could be explored using the protocols established here, which allow for the simultaneous detection of metabolic flux in multiple PDOs.

Bibliography

[1] Giuseppe Lippi and Camilla Mattiuzzi. “The global burden of pancreatic cancer”. In: *Archives of Medical Science : AMS* 16.4 (May 2020), pp. 820–824.

[2] S Lee. *Canadian Cancer Statistics*. 2022.

[3] Rebecca L. Siegel, Kimberly D. Miller, Hannah E. Fuchs, and Ahmedin Jemal. “Cancer statistics, 2022”. en. In: *CA: A Cancer Journal for Clinicians* 72.1 (2022). _eprint: https://onlinelibrary.wiley.com/doi/pdf/10.3322/caac.21708, pp. 7–33.

[4] Prashanth Rawla, Tagore Sunkara, and Vinaya Gaduputi. “Epidemiology of Pancreatic Cancer: Global Trends, Etiology and Risk Factors”. In: *World Journal of Oncology* 10.1 (Feb. 2019), pp. 10–27.

[5] Michael Orth, Philipp Metzger, et al. “Pancreatic ductal adenocarcinoma: biological hallmarks, current status, and future perspectives of combined modality treatment approaches”. In: *Radiation Oncology* 14.1 (Aug. 2019), p. 141.

[6] Capasso Mario, Franceschi Marilisa, et al. “Epidemiology and risk factors of pancreatic cancer”. In: *Acta Bio Medica : Atenei Parmensis* 89.Suppl 9 (2018), pp. 141–146.

[7] Vincent P. Groot, Neda Rezaee, et al. “Patterns, Timing, and Predictors of Recurrence Following Pancreatectomy for Pancreatic Ductal Adenocarcinoma”. en-US. In: *Annals of Surgery* 267.5 (May 2018), pp. 936–945.

[8] Daniel Schreyer, John P. Neoptolemos, Simon T. Barry, and Peter Bailey. “Deconstructing Pancreatic Cancer Using Next Generation-Omic Technologies–From

Discovery to Knowledge-Guided Platforms for Better Patient Management". In: *Frontiers in Cell and Developmental Biology* 9 (2022).

[9] Ashton A. Connor and Steven Gallinger. "Pancreatic cancer evolution and heterogeneity: integrating omics and clinical data". en. In: *Nature Reviews Cancer* 22.3 (Mar. 2022). Number: 3 Publisher: Nature Publishing Group, pp. 131–142.

[10] Cristoforo Grasso, Gerrit Jansen, and Elisa Giovannetti. "Drug resistance in pancreatic cancer: Impact of altered energy metabolism". en. In: *Critical Reviews in Oncology/Hematology* 114 (June 2017), pp. 139–152.

[11] Jakob Kirkegård, Frank Viborg Mortensen, and Deirdre Cronin-Fenton. "Chronic Pancreatitis and Pancreatic Cancer Risk: A Systematic Review and Meta-analysis". eng. In: *The American Journal of Gastroenterology* 112.9 (Sept. 2017), pp. 1366–1372.

[12] Donghui Li. "Diabetes and Pancreatic Cancer". In: *Molecular carcinogenesis* 51.1 (Jan. 2012), pp. 64–74.

[13] Anni M. Y. Zhang, Jamie Magrill, et al. *Endogenous insulin contributes to pancreatic cancer development*. en. Tech. rep. Section: New Results Type: article. bioRxiv, Jan. 2019, p. 530097.

[14] Anni M. Y. Zhang, Ken H. Chu, et al. "Effects of hyperinsulinemia on pancreatic cancer development and the immune microenvironment revealed through single-cell transcriptomics". In: *Cancer & Metabolism* 10 (Feb. 2022), p. 5.

[15] Phil A Hart, Melena D Bellin, et al. "Type 3c (pancreatogenic) diabetes mellitus secondary to chronic pancreatitis and pancreatic cancer". In: *The lancet. Gastroenterology & hepatology* 1.3 (Nov. 2016), pp. 226–237.

[16] Grainne M. O'Kane, Farah Ladak, and Steven Gallinger. "Advances in the management of pancreatic ductal adenocarcinoma". en. In: *CMAJ* 193.23 (June 2021). Publisher: CMAJ Section: Review, E844–E851.

[17] Benedikt Kaufmann, Daniel Hartmann, et al. "Neoadjuvant Treatment for Borderline Resectable Pancreatic Ductal Adenocarcinoma". In: *Digestive Surgery* 36.6 (2019). Publisher: Karger Publishers, pp. 455–461.

[18] Sonja Gillen, Tibor Schuster, et al. "Preoperative/Neoadjuvant Therapy in Pancreatic Cancer: A Systematic Review and Meta-analysis of Response and Resection Percentages". en. In: *PLOS Medicine* 7.4 (Apr. 2010). Publisher: Public Library of Science, e1000267.

[19] Gauri R. Varadhachary, Eric P. Tamm, et al. "Borderline resectable pancreatic cancer: definitions, management, and role of preoperative therapy". eng. In: *Annals of Surgical Oncology* 13.8 (Aug. 2006), pp. 1035–1046.

[20] Renata D'Alpino Peixoto, Caroline Speers, et al. "Prognostic factors and sites of metastasis in unresectable locally advanced pancreatic cancer". In: *Cancer Medicine* 4.8 (Aug. 2015), pp. 1171–1177.

[21] Eran van Veldhuisen, Claudia van den Oord, et al. "Locally Advanced Pancreatic Cancer: Work-Up, Staging, and Local Intervention Strategies". In: *Cancers* 11.7 (July 2019), p. 976.

[22] Andrew P. Loehrer and Cristina R. Ferrone. "Treatment of Locally Advanced Pancreatic Ductal Adenocarcinoma". In: *Digestive Surgery* 33.4 (2016). Publisher: Karger Publishers, pp. 343–350.

[23] Faiyaz Notta, Michelle Chan-Seng-Yue, et al. "A renewed model of pancreatic cancer evolution based on genomic rearrangement patterns". en. In: *Na-*

ture 538.7625 (Oct. 2016). Number: 7625 Publisher: Nature Publishing Group, pp. 378–382.

[24] M. Distler, D. Aust, et al. "Precursor Lesions for Sporadic Pancreatic Cancer: PanIN, IPMN, and MCN". en. In: *BioMed Research International* 2014 (Mar. 2014). Publisher: Hindawi, e474905.

[25] Lee Goldman. *Goldman-Cecil Medicine, 2-Volume Set, 25e*. 2015.

[26] Lena Haeberle and Irene Esposito. "Pathology of pancreatic cancer". In: *Translational Gastroenterology and Hepatology* 4 (June 2019), p. 50.

[27] Janel L. Kopp, Guido von Figura, et al. "Identification of Sox9-dependent acinar-to-ductal reprogramming as the principal mechanism for initiation of pancreatic ductal adenocarcinoma". In: *Cancer cell* 22.6 (Dec. 2012), pp. 737–750.

[28] Samra Turajlic, Andrea Sottoriva, Trevor Graham, and Charles Swanton. "Resolving genetic heterogeneity in cancer". en. In: *Nature Reviews Genetics* 20.7 (July 2019). Number: 7 Publisher: Nature Publishing Group, pp. 404–416.

[29] Benjamin J. Raphael, Ralph H. Hruban, et al. "Integrated Genomic Characterization of Pancreatic Ductal Adenocarcinoma". en. In: *Cancer Cell* 32.2 (Aug. 2017), 185–203.e13.

[30] Nicholas McGranahan and Charles Swanton. "Clonal Heterogeneity and Tumor Evolution: Past, Present, and the Future". en. In: *Cell* 168.4 (Feb. 2017), pp. 613–628.

[31] Takashi Murakami, Yukihiko Hiroshima, et al. "Role of the tumor microenvironment in pancreatic cancer". In: *Annals of Gastroenterological Surgery* 3.2 (Jan. 2019), pp. 130–137.

[32] Dagny von Ahrens, Tushar D. Bhagat, et al. “The role of stromal cancer-associated fibroblasts in pancreatic cancer”. In: *Journal of Hematology & Oncology* 10.1 (Mar. 2017), p. 76.

[33] Bolun Jiang, Li Zhou, et al. “Stroma-Targeting Therapy in Pancreatic Cancer: One Coin With Two Sides?” In: *Frontiers in Oncology* 10 (2020).

[34] Akio Yamasaki, Kosuke Yanai, and Hideya Onishi. “Hypoxia and pancreatic ductal adenocarcinoma”. en. In: *Cancer Letters* 484 (Aug. 2020), pp. 9–15.

[35] Berna C. Özdemir, Tsvetelina Pentcheva-Hoang, et al. “Depletion of carcinoma-associated fibroblasts and fibrosis induces immunosuppression and accelerates pancreas cancer with reduced survival”. eng. In: *Cancer Cell* 25.6 (June 2014), pp. 719–734.

[36] Andrew D. Rhim, Paul E. Oberstein, et al. “Stromal Elements Act to Restrain, Rather Than Support, Pancreatic Ductal Adenocarcinoma”. en. In: *Cancer Cell* 25.6 (June 2014), pp. 735–747.

[37] Jesse Gore and Murray Korc. “Pancreatic Cancer Stroma: Friend or Foe?” en. In: *Cancer Cell* 25.6 (June 2014), pp. 711–712.

[38] H. A. Burris, M. J. Moore, et al. “Improvements in survival and clinical benefit with gemcitabine as first-line therapy for patients with advanced pancreas cancer: a randomized trial”. eng. In: *Journal of Clinical Oncology: Official Journal of the American Society of Clinical Oncology* 15.6 (June 1997), pp. 2403–2413.

[39] Malcolm J. Moore, David Goldstein, et al. “Erlotinib plus gemcitabine compared with gemcitabine alone in patients with advanced pancreatic cancer: a phase III trial of the National Cancer Institute of Canada Clinical Trials Group”. eng. In: *Journal of Clinical Oncology: Official Journal of the American Society of Clinical Oncology* 25.15 (May 2007), pp. 1960–1966.

[40] Thierry Conroy, Françoise Desseigne, et al. “FOLFIRINOX versus gemcitabine for metastatic pancreatic cancer”. eng. In: *The New England Journal of Medicine* 364.19 (May 2011), pp. 1817–1825.

[41] Daniel D. Von Hoff, Thomas Ervin, et al. “Increased survival in pancreatic cancer with nab-paclitaxel plus gemcitabine”. eng. In: *The New England Journal of Medicine* 369.18 (Oct. 2013), pp. 1691–1703.

[42] Andrea Wang-Gillam, Chung-Pin Li, et al. “Nanoliposomal irinotecan with fluorouracil and folinic acid in metastatic pancreatic cancer after previous gemcitabine-based therapy (NAPOLI-1): a global, randomised, open-label, phase 3 trial”. English. In: *The Lancet* 387.10018 (Feb. 2016). Publisher: Elsevier, pp. 545–557.

[43] Talia Golan, Pascal Hammel, et al. “Maintenance Olaparib for Germline BRCA-Mutated Metastatic Pancreatic Cancer”. In: *New England Journal of Medicine* 381.4 (July 2019). Publisher: Massachusetts Medical Society _eprint: https://doi.org/10.1056/NEJMoa1903387, pp. 317–327.

[44] D. J. Renouf, J. J. Knox, et al. “LBA65 The Canadian Cancer Trials Group PA.7 trial: Results of a randomized phase II study of gemcitabine (GEM) and nab-paclitaxel (Nab-P) vs GEM, nab-P, durvalumab (D) and tremelimumab (T) as first line therapy in metastatic pancreatic ductal adenocarcinoma (mPDAC)”. English. In: *Annals of Oncology* 31 (Sept. 2020). Publisher: Elsevier, S1195.

[45] Eva Versteijne, Jacob L. van Dam, et al. “Neoadjuvant Chemoradiotherapy Versus Upfront Surgery for Resectable and Borderline Resectable Pancreatic Cancer: Long-Term Results of the Dutch Randomized PREOPANC Trial”. In: *Journal of Clinical Oncology* (Jan. 2022). Publisher: Wolters Kluwer, JCO.21.02233.

[46] Fausto Petrelli, Andrea Coinu, et al. “FOLFIRINOX-Based Neoadjuvant Therapy in Borderline Resectable or Unresectable Pancreatic Cancer: A Meta-Analytical Review of Published Studies”. en-US. In: *Pancreas* 44.4 (May 2015), pp. 515–521.

[47] Paul C. McDonald, Stephen Chia, et al. “A Phase 1 Study of SLC-0111, a Novel Inhibitor of Carbonic Anhydrase IX, in Patients With Advanced Solid Tumors”. en-US. In: *American Journal of Clinical Oncology* 43.7 (July 2020), pp. 484–490.

[48] Eric A. Collisson, Anguraj Sadanandam, et al. “Subtypes of pancreatic ductal adenocarcinoma and their differing responses to therapy”. en. In: *Nature Medicine* 17.4 (Apr. 2011). Number: 4 Publisher: Nature Publishing Group, pp. 500–503.

[49] Anneleen Daemen, David Peterson, et al. “Metabolite profiling stratifies pancreatic ductal adenocarcinomas into subtypes with distinct sensitivities to metabolic inhibitors”. In: *Proceedings of the National Academy of Sciences* 112.32 (2015), E4410–E4417.

[50] Yongxing Du, Bangbo Zhao, et al. “Molecular Subtyping of Pancreatic Cancer: Translating Genomics and Transcriptomics into the Clinic”. In: *Journal of Cancer* 8.4 (Feb. 2017), pp. 513–522.

[51] Richard A. Moffitt, Raoud Marayati, et al. “Virtual microdissection identifies distinct tumor- and stroma-specific subtypes of pancreatic ductal adenocarcinoma”. en. In: *Nature Genetics* 47.10 (Oct. 2015). Number: 10 Publisher: Nature Publishing Group, pp. 1168–1178.

[52] Peter Bailey, David K. Chang, et al. “Genomic analyses identify molecular subtypes of pancreatic cancer”. en. In: *Nature* 531.7592 (Mar. 2016). Number: 7592 Publisher: Nature Publishing Group, pp. 47–52.

[53] Francesco Puleo, Rémy Nicolle, et al. “Stratification of Pancreatic Ductal Adenocarcinomas Based on Tumor and Microenvironment Features”. en. In: *Gastroenterology* 155.6 (Dec. 2018), 1999–2013.e3.

[54] Eric A. Collisson, Peter Bailey, David K. Chang, and Andrew V. Biankin. “Molecular subtypes of pancreatic cancer”. en. In: *Nature Reviews Gastroenterology & Hepatology* 16.4 (Apr. 2019). Number: 4 Publisher: Nature Publishing Group, pp. 207–220.

[55] Ronnie Ren Jie Low, Wei Wen Lim, et al. “The Diverse Applications of Pancreatic Ductal Adenocarcinoma Organoids”. en. In: *Cancers* 13.19 (Jan. 2021). Number: 19 Publisher: Multidisciplinary Digital Publishing Institute, p. 4979.

[56] Hiromitsu Hayashi, Takaaki Higashi, et al. “Recent advances in precision medicine for pancreatic ductal adenocarcinoma”. en. In: *Annals of Gastroenterological Surgery* 5.4 (2021). _eprint: https://onlinelibrary.wiley.com/doi/pdf/10.1002/ags3.12436, pp. 457–466.

[57] Changyong Wei, Monique Heitmeier, Paul W. Hruz, and Mala Shanmugam. “Evaluating the Efficacy of GLUT Inhibitors Using a Seahorse Extracellular Flux Analyzer”. eng. In: *Methods in Molecular Biology (Clifton, N.J.)* 1713 (2018), pp. 69–75.

[58] Maria V. Liberti and Jason W. Locasale. “The Warburg Effect: How Does it Benefit Cancer Cells?” en. In: *Trends in biochemical sciences* 41.3 (Mar. 2016). Publisher: NIH Public Access, p. 211.

[59] Leonardo M. R. Ferreira, Albert M. Li, et al. “Intermediary metabolism: An intricate network at the crossroads of cell fate and function”. en. In: *Biochimica et Biophysica Acta (BBA) - Molecular Basis of Disease* 1866.10 (Oct. 2020), p. 165887.

[60] Chang Liu, Ying Jin, and Zhimin Fan. “The Mechanism of Warburg Effect-Induced Chemoresistance in Cancer”. In: *Frontiers in Oncology* 11 (2021).

[61] Q. Cai, T. Lin, S. Kamarajugadda, and J. Lu. “Regulation of glycolysis and the Warburg effect by estrogen-related receptors”. en. In: *Oncogene* 32.16 (Apr. 2013). Number: 16 Publisher: Nature Publishing Group, pp. 2079–2086.

[62] Lan Zhao, Hongya Zhao, and Hong Yan. “Gene expression profiling of 1200 pancreatic ductal adenocarcinoma reveals novel subtypes”. In: *BMC Cancer* 18 (May 2018), p. 603.

[63] Pilar Espiau-Romera, Sarah Courtois, Beatriz Parejo-Alonso, and Patricia Sancho. “Molecular and Metabolic Subtypes Correspondence for Pancreatic Ductal Adenocarcinoma Classification”. In: *Journal of Clinical Medicine* 9.12 (Dec. 2020), p. 4128.

[64] Joanna M. Karasinska, James T. Topham, et al. “Altered Gene Expression along the Glycolysis–Cholesterol Synthesis Axis Is Associated with Outcome in Pancreatic Cancer”. In: *Clinical Cancer Research* 26.1 (Jan. 2020), pp. 135–146.

[65] “UniProt: the universal protein knowledgebase in 2021”. In: *Nucleic acids research* 49.D1 (2021), pp. D480–D489.

[66] Eunjin Koh, Young Kyung Kim, Daye Shin, and Kyung-Sup Kim. “MPC1 is essential for PGC-1α-induced mitochondrial respiration and biogenesis”. In: *Biochemical Journal* 475.10 (May 2018), pp. 1687–1699.

[67] Benoît Vanderperre, Tom Bender, Edmund RS Kunji, and Jean-Claude Martinou. “Mitochondrial pyruvate import and its effects on homeostasis”. en. In: *Current Opinion in Cell Biology*. Cell regulation 33 (Apr. 2015), pp. 35–41.

[68] Tom Bender and Jean-Claude Martinou. “The mitochondrial pyruvate carrier in health and disease: To carry or not to carry?” en. In: *Biochimica et Biophysica Acta (BBA) - Molecular Cell Research*. Channels and transporters in cell metabolism 1863.10 (Oct. 2016), pp. 2436–2442.

[69] *PubChem Pathway Summary for Pathway R-HSA-71406*.

[70] Chaoqun Wang, Liqian Dong, et al. “The PGC1α/NRF1-MPC1 axis suppresses tumor progression and enhances the sensitivity to sorafenib/doxorubicin treatment in hepatocellular carcinoma”. en. In: *Free Radical Biology and Medicine* 163 (Feb. 2021), pp. 141–152.

[71] Yuji Takaoka, Masamitsu Konno, et al. “Mitochondrial pyruvate carrier 1 expression controls cancer epithelial-mesenchymal transition and radioresistance”. eng. In: *Cancer Science* 110.4 (Apr. 2019), pp. 1331–1339.

[72] Yi Chai, Caixia Wang, et al. “MPC1 deletion is associated with poor prognosis and temozolomide resistance in glioblastoma”. en. In: *Journal of Neuro-Oncology* 144.2 (Sept. 2019), pp. 293–301.

[73] Javier Traba, Pietro Miozzo, et al. “An Optimized Protocol to Analyze Glycolysis and Mitochondrial Respiration in Lymphocytes”. In: *Journal of Visualized Experiments : JoVE* 117 (Nov. 2016), p. 54918.

[74] Wantong Yao, Anirban Maitra, and Haoqiang Ying. “Recent insights into the biology of pancreatic cancer”. In: *EBioMedicine* 53 (Mar. 2020), p. 102655.

[75] Erin Pleasance, Emma Titmuss, et al. “Pan-cancer analysis of advanced patient tumors reveals interactions between therapy and genomic landscapes”. en. In: *Nature Cancer* 1.4 (Apr. 2020). Number: 4 Publisher: Nature Publishing Group, pp. 452–468.

[76] Heng Li and Richard Durbin. “Fast and accurate short read alignment with Burrows–Wheeler transform”. In: *Bioinformatics* 25.14 (July 2009), pp. 1754–1760.

[77] Artem Tarasov, Albert J. Vilella, et al. “Sambamba: fast processing of NGS alignment formats”. eng. In: *Bioinformatics (Oxford, England)* 31.12 (June 2015), pp. 2032–2034.

[78] Alexander Dobin, Carrie A. Davis, et al. “STAR: ultrafast universal RNA-seq aligner”. In: *Bioinformatics* 29.1 (Jan. 2013), pp. 15–21.

[79] Yang Liao, Gordon K. Smyth, and Wei Shi. “featureCounts: an efficient general purpose program for assigning sequence reads to genomic features”. eng. In: *Bioinformatics (Oxford, England)* 30.7 (Apr. 2014), pp. 923–930.

[80] *Seahorse XFe96 Analyzer*.

[81] Chiara Magliaro, Andrea Rinaldo, and Arti Ahluwalia. “Allometric Scaling of physiologically-relevant organoids”. In: *Scientific Reports* 9 (Aug. 2019), p. 11890.

[82] Atena Malakpour-Permlid and Stina Oredsson. “A novel 3D polycaprolactone high-throughput system for evaluation of toxicity in normoxia and hypoxia”. eng. In: *Toxicology Reports* 8 (2021), pp. 627–635.

[83] *XFe96 cell culture microplates*. 2022.

[84] *Corning Matrigel Matrix High Concentration*. 2022.

[85] Paul M. Hinderliter, Kevin R. Minard, et al. “ISDD: A computational model of particle sedimentation, diffusion and target cell dosimetry for in vitro toxicity studies”. In: *Particle and Fibre Toxicology* 7.1 (Nov. 2010), p. 36.

[86] Lindsey A. Baker, Hervé Tiriac, Hans Clevers, and David A. Tuveson. “Modeling pancreatic cancer with organoids”. In: *Trends in cancer* 2.4 (Apr. 2016), pp. 176–190.

[87] Jindrich Symersky, Daniel Osowski, D Eric Walters, and David M Mueller. "Oligomycin frames a common drug-binding site in the ATP synthase". In: *Proceedings of the National Academy of Sciences* 109.35 (2012), pp. 13961–13965.

[88] Mihir N. Nakrani, Robert H. Wineland, and Fatima Anjum. "Physiology, Glucose Metabolism". eng. In: *StatPearls*. Treasure Island (FL): StatPearls Publishing, 2022.

[89] Mayo Foundation for Medical Education and Research. 2022.

[90] Andrew P Halestrap. "The mitochondrial pyruvate carrier. Kinetics and specificity for substrates and inhibitors". In: *Biochemical Journal* 148.1 (1975), pp. 85–96.

[91] Nathaniel M Vacanti, Ajit S Divakaruni, et al. "Regulation of substrate utilization by the mitochondrial pyruvate carrier". In: *Molecular cell* 56.3 (2014), pp. 425–435.

[92] Shane R Solst, Samuel N Rodman, et al. "141 - Inhibition of Mitochondrial Pyruvate Transport Selectively Sensitizes Cancer Cells to Metabolic Oxidative Stress". en. In: *Free Radical Biology and Medicine*. SfRBM 2017 SfRBM's 24th Annual Meeting Program and Abstracts November 29 - December 2, 2017 Hilton Baltimore Baltimore, MD USA 112 (Nov. 2017), p. 102.

[93] Sarah J Mitchell, Alejandro Martin-Montalvo, et al. "The SIRT1 activator SRT1720 extends lifespan and improves health of mice fed a standard diet". In: *Cell reports* 6.5 (2014), pp. 836–843.

[94] Fengxia Liang, Shinji Kume, and Daisuke Koya. "SIRT1 and insulin resistance". en. In: *Nature Reviews Endocrinology* 5.7 (July 2009). Number: 7 Publisher: Nature Publishing Group, pp. 367–373.

[95] Yang Zhou, Shaohua Wang, et al. “SIRT1/PGC-1α Signaling Promotes Mitochondrial Functional Recovery and Reduces Apoptosis after Intracerebral Hemorrhage in Rats”. In: *Frontiers in Molecular Neuroscience* 10 (Jan. 2018), p. 443.

[96] Sunghee Park, Rachid Safi, et al. “Inhibition of ERRα Prevents Mitochondrial Pyruvate Uptake Exposing NADPH-Generating Pathways as Targetable Vulnerabilities in Breast Cancer”. en. In: *Cell Reports* 27.12 (June 2019), 3587–3601.e4.

[97] Xingxing Kong, Rui Wang, et al. “Sirtuin 3, a new target of PGC-1alpha, plays an important role in the suppression of ROS and mitochondrial biogenesis”. eng. In: *PloS One* 5.7 (July 2010), e11707.

[98] Jasmine George and Nihal Ahmad. “Mitochondrial sirtuins in cancer: Emerging roles and therapeutic potential”. In: *Cancer research* 76.9 (May 2016), pp. 2500–2506.

[99] Yang-Yi Fan, Laurie A. Davidson, et al. “A bioassay to measure energy metabolism in mouse colonic crypts, organoids, and sorted stem cells”. In: *American Journal of Physiology - Gastrointestinal and Liver Physiology* 309.1 (July 2015), G1–G9.

[100] Alexander Ioannis Damanakis, Florian Gebauer, Felix Popp, and Christiane Bruns. “The Hallmarks of Pancreatic Cancer”. en. In: *Textbook of Pancreatic Cancer: Principles and Practice of Surgical Oncology*. Ed. by Kjetil Søreide and Stefan Stättner. Cham: Springer International Publishing, 2021, pp. 189–201.

[101] T. Miura and R. Tanaka. “*In vitro* Vasculogenesis Models Revisited - Measurement of VEGF Diffusion in Matrigel”. en. In: *Mathematical Modelling of Natural Phenomena* 4.4 (2009), pp. 118–130.

[102] Y.-C. Shen, D.-L. Ou, et al. "Activating oxidative phosphorylation by a pyruvate dehydrogenase kinase inhibitor overcomes sorafenib resistance of hepatocellular carcinoma". en. In: *British Journal of Cancer* 108.1 (Jan. 2013). Number: 1 Publisher: Nature Publishing Group, pp. 72–81.

[103] Mengqi Liu, Wensheng Liu, et al. "Regulation of metabolic reprogramming by tumor suppressor genes in pancreatic cancer". In: *Experimental Hematology & Oncology* 9.1 (Sept. 2020), p. 23.

[104] Yumin Hu, Weiqin Lu, et al. "K-rasG12V transformation leads to mitochondrial dysfunction and a metabolic switch from oxidative phosphorylation to glycolysis". en. In: *Cell Research* 22.2 (Feb. 2012). Number: 2 Publisher: Nature Publishing Group, pp. 399–412.

[105] Alexander A. Shestov, Xiaojing Liu, et al. "Quantitative determinants of aerobic glycolysis identify flux through the enzyme GAPDH as a limiting step". eng. In: *eLife* 3 (July 2014).

[106] Kaiyan Liu, Zhenjie Tang, et al. "Glyceraldehyde-3-phosphate dehydrogenase promotes cancer growth and metastasis through upregulation of SNAIL expression". In: *International Journal of Oncology* 50.1 (Jan. 2017). Publisher: Spandidos Publications, pp. 252–262.

[107] Nana-Maria Grüning, Dijun Du, et al. "Inhibition of triosephosphate isomerase by phosphoenolpyruvate in the feedback-regulation of glycolysis". In: *Open Biology* 4.3 (Mar. 2014), p. 130232.

[108] Tingting Chen, Zhigang Huang, et al. "Clinical significance and prognostic value of Triosephosphate isomerase expression in gastric cancer". In: *Medicine* 96.19 (May 2017), e6865.

[109] Tomás Duraj, Josefa Carrión-Navarro, et al. “Metabolic therapy and bioenergetic analysis: The missing piece of the puzzle”. en. In: *Molecular Metabolism* 54 (Dec. 2021), p. 101389.

[110] Shona A. Mookerjee and Martin D. Brand. “Measurement and Analysis of Extracellular Acid Production to Determine Glycolytic Rate”. In: *Journal of Visualized Experiments : JoVE* 106 (Dec. 2015), p. 53464.

[111] Leiming Wang, Mafei Xu, et al. “MPC1, a key gene in cancer metabolism, is regulated by COUPTFII in human prostate cancer”. In: *Oncotarget* 7.12 (Feb. 2016), pp. 14673–14683.

[112] John C. Schell, Kristofor A. Olson, et al. “A Role for the Mitochondrial Pyruvate Carrier as a Repressor of the Warburg Effect and Colon Cancer Cell Growth”. en. In: *Molecular Cell* 56.3 (Nov. 2014), pp. 400–413.

[113] John C. Schell, Dona R. Wisidagama, et al. “Control of intestinal stem cell function and proliferation by mitochondrial pyruvate metabolism”. In: *Nature cell biology* 19.9 (Sept. 2017), pp. 1027–1036.

[114] Liang Xu, Clyde F. Phelix, and Liao Y. Chen. “Structural Insights into the Human Mitochondrial Pyruvate Carrier Complexes”. en. In: *Journal of Chemical Information and Modeling* (Oct. 2021). Publisher: American Chemical Society.

[115] Florencia García-Campusano, Víctor-Hugo Anaya, et al. “ALT1-encoded alanine aminotransferase plays a central role in the metabolism of alanine in Saccharomyces cerevisiae”. eng. In: *Canadian Journal of Microbiology* 55.4 (Apr. 2009), pp. 368–374.

[116] Ainhoa Ruiz-Iglesias and Santos Mañes. “The Importance of Mitochondrial Pyruvate Carrier in Cancer Cell Metabolism and Tumorigenesis”. en. In: *Can-*

cers 13.7 (Jan. 2021). Number: 7 Publisher: Multidisciplinary Digital Publishing Institute, p. 1488.

[117] Karasinska. *Prognostic metabolic signatures in pancreatic ductal adenocarcinoma - Poster - USCAP*. 2008.

[118] Jessica D. Panes, Pamela A. Godoy, et al. "Changes in PGC-1α/SIRT1 Signaling Impact on Mitochondrial Homeostasis in Amyloid-Beta Peptide Toxicity Model". In: *Frontiers in Pharmacology* 11 (2020).

[119] Jihye Yun, Edouard Mullarky, et al. "Vitamin C selectively kills KRAS and BRAF mutant colorectal cancer cells by targeting GAPDH". eng. In: *Science (New York, N.Y.)* 350.6266 (Dec. 2015), pp. 1391–1396.

Appendices

A1 Appendix Figures

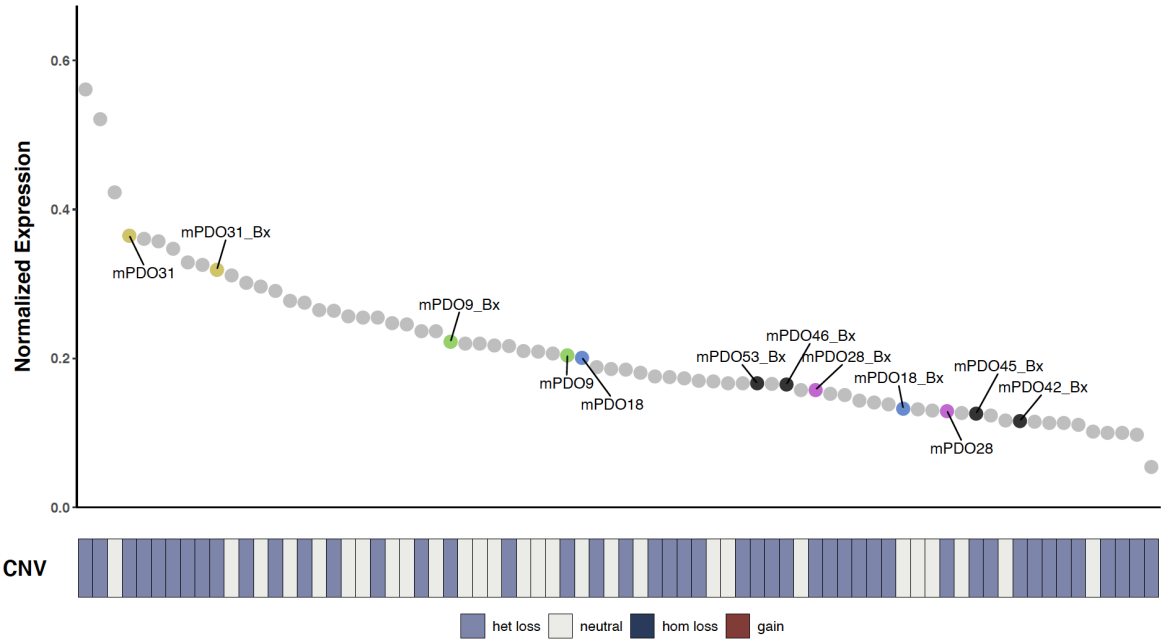

Figure A.1: Comparing MPC1 expression between PDO and Biopsy